This is to certify that the

thesis entitled

AN AIR MASS CLIMATOLOGY FOR NORTHWEST OHIO BASED ON AIRFLOW TRAJECTORIES

presented by

Eleanor A. Waller

has been accepted towards fulfillment
of the requirements for

M.A. degree in Geography

Julie A. Winkler
Major professor

Date May 3, 1999

AN AIR MASS CLIMATOLOGY FOR NORTHWEST OHIO BASED ON AIRFLOW TRAJECTORIES

By

Eleanor A. Waller

A THESIS

Submitted to
Michigan State University
in partial fulfillment of the requirements
for the degree of

MASTER OF ARTS

Department of Geography

1999

ABSTRACT

AN AIR MASS CLIMATOLOGY FOR NORTHWEST OHIO BASED ON AIRFLOW TRAJECTORIES

By

Eleanor A. Waller

An air mass climatology was prepared for a location in northwest Ohio using the method of trajectory analysis. For a ten year period,1976-1985, 5-day isobaric back-trajectories terminating at the study site were calculated in 6-hour intervals twice-daily at the 850 mb pressure level and aggregated by month. A grid-based approach known as residence-time analysis, implemented with a raster GIS, was used to analyze the spatial distribution of the gridded 6-hour trajectory node frequencies. The monthly spatial distribution of the gridded trajectory node frequencies illuminated numerous airflow corridors which displayed both geographic and seasonal preferences. The most distinct airflow corridor, present in most months except September and October, is a north-northwesterly corridor. Canadian and Arctic air masses, transported by this corridor and a northwesterly airflow corridor, were the most frequent air mass types in all seasons. In general, this work found considerably less evidence of tropical air masses in all seasons than previous authors. Also, the results of the study suggest that Pacific and southwest air masses are more frequent than previously thought.

ACKNOWLEDGMENTS

This thesis would not have been possible without the help of some very important people. I would like first of all to thank my advisor, Dr. Julie Winkler, for her encouragement and support throughout my master's program, for her guidance in this research effort, and for the countless hours spent reviewing this work. It has been a privilege to work with such a dedicated researcher. I would also like to thank Drs. Jay Harman and Daniel Brown for their guidance and their many helpful suggestions in this research and also for their excellent teaching skills. My most important thanks go to my husband Vinij, my children, Joey and Kristi, and my parents, Franz and Hildegard Waller, for their patience and support throughout this long effort. Without their loving support, this effort would surely have been much more difficult.

TABLE OF CONTENTS

LIST OF TABLES

LIST OF FIGURES

CHAPTER I

INTRODUCTION, LITERATURE REVIEW AND OBJECTIVES

1. Overview

An air mass is generally defined as "a large body of air with relatively homogeneous temperature, humidity, and lapse rate across its horizontal extent" (Corcoran, 1987). The concept of air masses and their role in the climatology of the middle latitudes was first developed in the early part of this century by V. Bjerknes, J. Bjerknes and T. Bergeron and colleagues (Bjerknes, 1921; Bergeron, 1928; Bergeron, 1930). Typically, air masses form within semi-permanent anticyclonic circulation systems (i.e., high-pressure systems) over relatively homogeneous surfaces (Bergeron, 1928). As an air mass develops, it acquires the temperature and moisture properties of the surface over which it is located. Examples of air mass source regions include the high latitude ice-covered expanses of North America during the winter and the subtropical oceans at all times of the year (Willett, 1933). Lower and mid tropospheric airflow can steer air masses out of their regions of origin and into the middle latitudes.

The frequency of different types of air masses is an important element in understanding the climate of the middle latitudes, and air mass climatologies have been constructed for North America and/or sub-regions within North America (Brunnschweiler, 1952; Bryson, 1966; Schwartz, 1982; Schwartz et al.,

1985; Schwartz, 1991), as well as for other parts of the world (see Corcoran (1987) for a review). According to Corcoran (1987), an air mass climatology "will describe the types of air masses found in an area, will classify them according to their characteristics, and will determine their seasonal or annual frequency of occurrence".

Some authors have based their air mass classification schemes exclusively on the temperature and moisture properties of air masses (e.g., Willett, 1933; Schwartz, 1982). There are many recognized difficulties with this approach, not the least of which is the rather subjective establishment of the numerical limits of the temperature and moisture parameters for each air mass type. Identifying appropriate numerical limits is a complex problem since: 1) original air mass properties are modified by the underlying surface as the air mass moves out of its region of origin, and 2) these properties also change on a seasonal basis.

The difficulties in defining air masses have lead some researchers to consider trajectory analysis as an alternative methodology. In some cases, trajectories were used only to supplement methodologies based primarily on temperature and moisture conditions (e.g., Brunnschweiler, 1952; Bryson, 1966), whereas other studies have focused exclusively on airflow in determining air mass source regions (e.g., Bryson, 1966; Wendland and Bryson, 1981; Wendland and McDonald, 1986). Focusing exclusively on airflow eliminates the need to define temperature and moisture limits for an air mass type. This

approach is able to identify source regions of air masses as well as the movement after leaving their regions of origin.

The calculation of airflow trajectories, however, is computationally intense and the display, integration and interpretation of trajectories are cumbersome and difficult, particularly as hundreds or even thousands of trajectories are typically required for climatological analysis. Typical trajectory plots, often referred to as "spaghetti maps", are not well suited for climatological analysis as the curving trajectories are typically overlaid and displayed together. It is difficult to discern from these spaghetti maps the "common or typical" pattern, a goal of climatological analysis. Also, many of the computer models developed to calculate trajectory analysis have, until recently, been expensive to use, as most of these models could not be run on personal computers. Furthermore, these computer models may not be directly applicable for climatological studies of air masses, as they were originally developed for a quite different purpose -- that is, to investigate episodic long-range transport and deposition of air pollutants.

Recent advances in personal computer technology, along with improved analysis and display software such as geographic information systems (GIS), provide new opportunities for constructing air mass climatologies based on trajectory analysis. In this thesis, display and interpretation methods for trajectory analysis are developed and then employed to prepare an air mass climatology for northwest Ohio. Northwest Ohio was chosen as the study area as previous studies (e.g., Wendland and Bryson, 1986; Schwartz, 1982) suggest

that this region experiences a number of different air mass types during a typical year. Besides providing an updated air mass climatology, the trajectory analyses presented here have obvious applications for other disciplines, as well. For example, northwest Ohio is in a region which is frequently cited as being either a pathway or source of atmospheric pollutants (Wolff et al., 1984; Poirot and Wishinski, 1986; Comrie, 1994). Northwest Ohio is also an important agricultural area that can be affected by airborne plant diseases (Davis and Main, 1984), and insect pests that are transported into the region from "overwintering" sites in the southern United States (Carlson et al., 1992).

2. Literature Review

In this section, previous literature relevant to this study is reviewed. The review is organized into two parts. The first part deals with airflow analysis techniques and their uses in climatology. The second part deals with previous air mass climatologies of North America in order to provide a background for comparing the results of this study to those of previous studies.

a. Techniques previously employed for analyzing airflow

1) METHODS BASED ON THE INSTANTANEOUS WIND

Wind roses, wind vectors, and streamlines are commonly-used tools for describing the mean airflow conditions of a region or place. All three are methods of analyzing the "instantaneous" wind, or, in other words, the wind

measured at a specific time and location. Wind roses typically display the relative frequency of the instantaneous wind direction by direction category. The direction categories are usually centered on the cardinal compass points. In climatological analysis, a wind rose is usually prepared for individual sites, and generally represents the frequency of the wind by direction over an extended period (say 30 years) for a specified time interval (the month of March, for example). As an example, the *Climatological Atlas of the United States* (Department of Commerce, 1968; pp. 75-78) provides wind roses by month and for the year as a whole based on ten years of data (1951-1960) at numerous locations across the U.S. Another example (Figure 1) is from Winkler et al. (1996), where wind roses were used to depict different aspects of the average lower tropospheric wind (i.e. frequency, speed, and wind run) by compass direction using a 16-compass-point rose.

Wind vectors are commonly used to represent the directionality and velocity of airflow. An arrow is drawn such that the arrow points in the direction to which the wind is blowing, and the length of the arrow shaft is proportional to the speed of the wind. For climatological analysis, usually the resultant rather than the actual wind vector is displayed. The resultant wind vector is the vectorial average of the u (east-west) and v (north-south) components of the instantaneous wind, summed separately over a given time period. The averaged wind components are then converted using simple geometry into a single vector, known as the resultant wind vector. Again, as an example, mean resultant wind

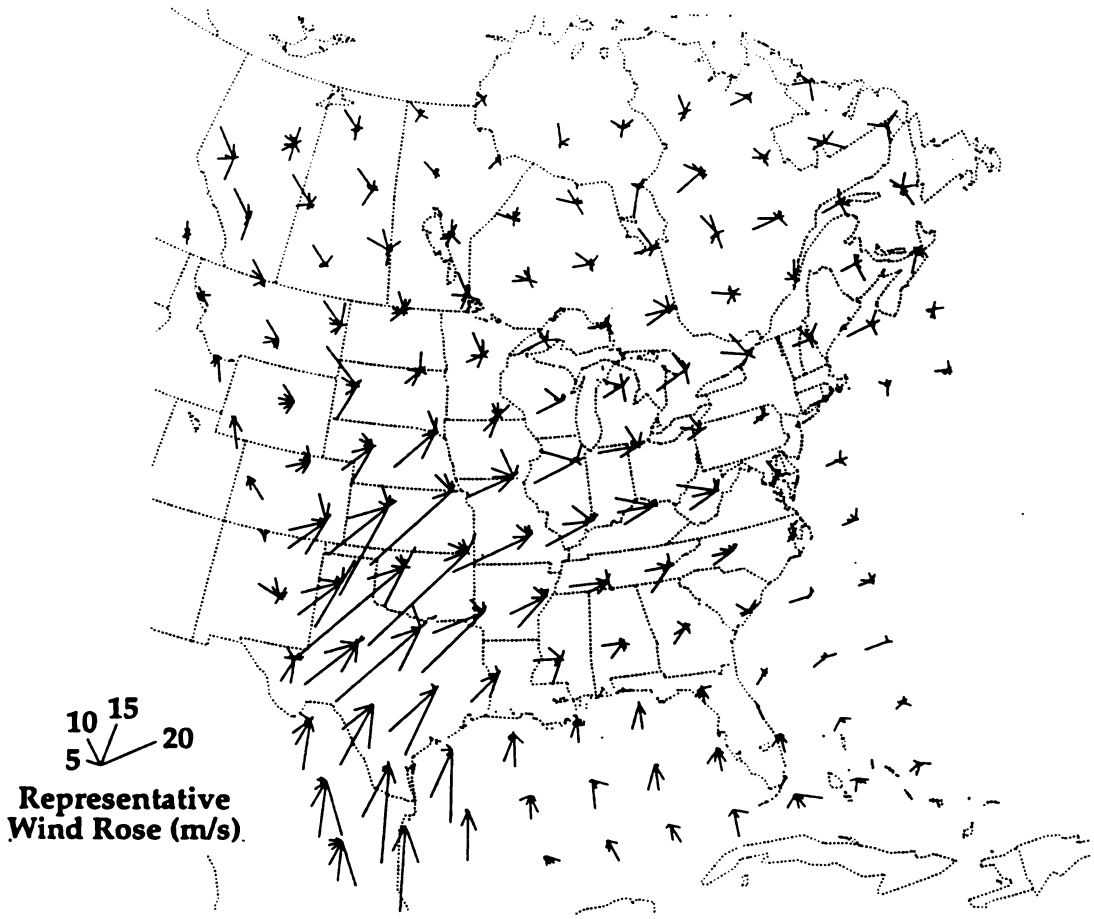

Figure 1. An example of a wind rose map (from Winkler et al., 1996).

vectors were used by Winkler et al. (1996) (Figure 2) to depict the average wind for each of the spring months (1969-1989) at gridpoint locations over central and eastern North America in the lower troposphere. Wind vectors can also be found in the *Climatological Atlas of the United States* (Department of Commerce, 1968, p. 78) where mid-seasonal (i.e., the months of January, April, July, October)

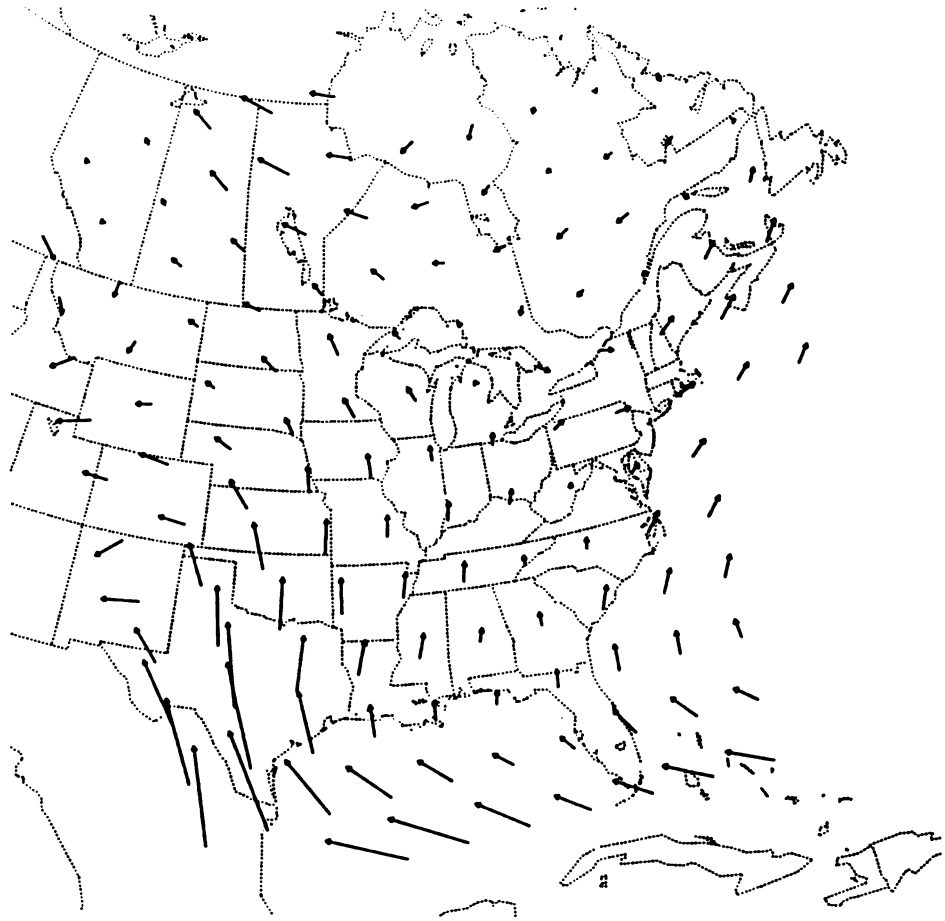

Figure 2. An example of a wind vector map (from Winkler et al., 1996).

maps of resultant wind vectors were based on hourly observations for ten years (1951-1960).

Streamline analysis is another method for depicting the instantaneous airflow over a broad horizontal area. Streamlines are a set of lines that are drawn parallel to the wind vectors at a particular atmospheric level (Wallace and

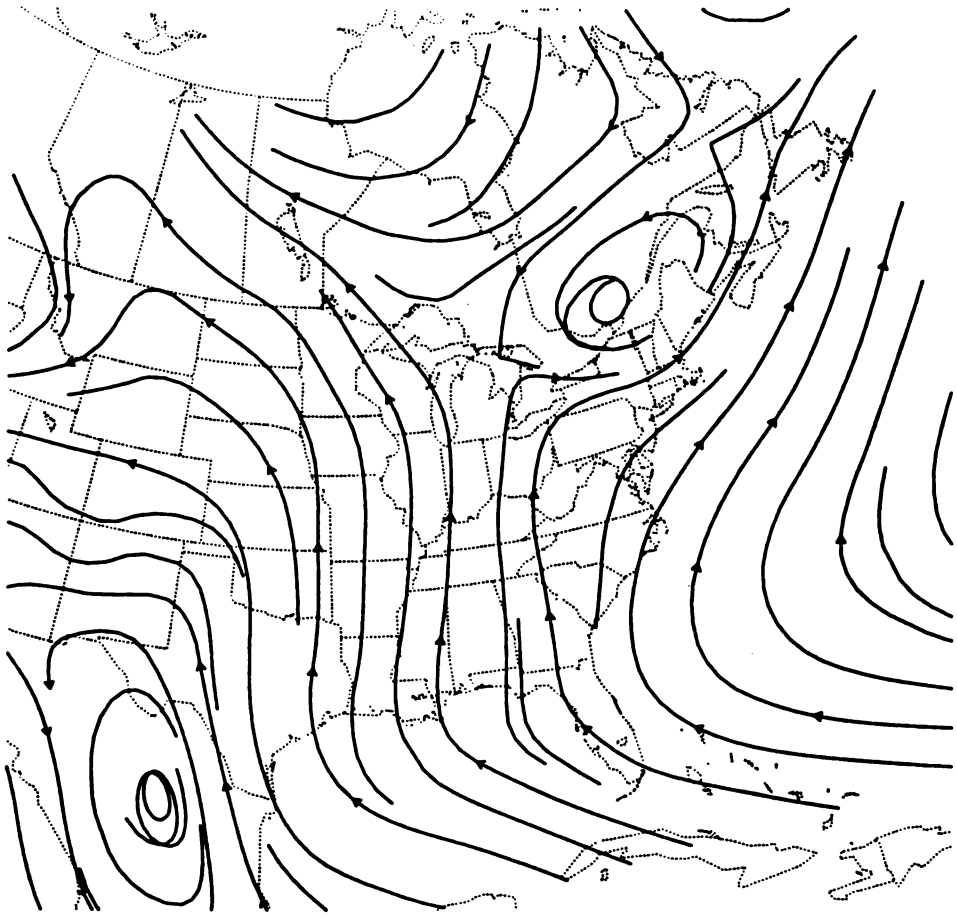

Figure 3. An example of a streamline analysis map (from Winkler et al., 1996).

Hobbs, 1977; p. 364). In climatological analysis, streamlines are usually drawn from the resultant wind vectors. An example is the streamline plots by Winkler et al. (1996) used to depict average airflow for the springtime lower troposphere over central and eastern North America (Figure 3). The streamlines were based on resultant wind vectors calculated from 21 years (1969-1989) of wind .

observations. Streamlines are particularly useful in identifying zones of converging and diverging airflow (Ahrens, 1994, p. 430) and have been used by a number of authors to study air masses and their source regions (Borchert, 1950; Bryson, 1966; Wendland and Bryson, 1981; Wendland and McDonald, 1986). According to Wendland and Bryson (1981), convergence of resultant wind streamlines corresponds to areas between or separating air mass source regions, whereas divergence zones identify areas where air masses frequently develop.

2) TRAJECTORY ANALYSIS

(i) Definition

Wind roses, wind vectors and streamlines do not show the actual path of an air parcel or air mass. This is because they do not take into account translation of weather systems or the strengthening and weakening of systems. The effect of system movement on streamlines and trajectories is illustrated in Figure 4. Depicted are two sets of instantaneous streamlines illustrating the eastward propagation of a wave at an initial time (thin solid lines), and at some later time (dashed lines). The heavy arrows represent horizontal airflow trajectories originating at point A that were created under different horizontal wind speeds. When the wind speed at point A is faster than the propagation of the wave, trajectory AB occurs. Note that this is the longest trajectory as it was obtained from the strongest wind. On the other hand, trajectory AD occurs when

the wind speed at point A is slower than the wave propagation speed. These two trajectories illustrate how the curvature of airflow trajectories and streamlines is usually quite different. The only condition which allows the trajectory and the streamline to follow the same path in time is when the wind speed at point A is exactly equal to the rate of wave propagation, shown by trajectory AC.

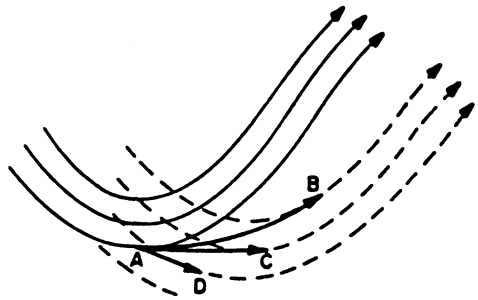

Figure 4. Streamlines versus trajectories. The heavy arrows depict airflow trajectories, thin arrows depict earlier streamlines and dashed arrows depict later streamlines (from Wallace and Hobbs, 1977; p. 381).

Trajectories are an ideal tool for analyzing the origin or destination of air parcels and/or air masses. An airflow trajectory, by definition, is "the actual path that an air parcel follows as it moves through space" (Wallace and Hobbs, 1977; p. 381). To retrace the path of an air parcel, a time series of wind observations over a broad horizontal and vertical area is used to calculate earlier upwind locations at regular time intervals beginning at a particular site. This type of an airflow trajectory is known as a back trajectory. Trajectories can also be calculated forward in time to identify downwind locations of the air parcel. In

both cases, the resulting trajectory resembles a curving line with nodes that indicate locations at fixed time intervals along the path. Figure 5 is an example of a single airflow trajectory. The distance between the nodes in a trajectory is a

Figure 5. An example of a single back trajectory. Plus-signs mark the terminus and 6-hour nodes.

function of the strength of the wind. The maximum length of a trajectory is ultimately dependent on the spatial and temporal extent of the meteorological data set that is being used. A long trajectory (in terms of days or hours) is necessary to indicate the general vicinity of the source region for air masses affecting mid-latitude locations.

Backward trajectories have been used in a number of climatological analyses (e.g., Bryson, 1966; Miller, 1981a, 1981b; Miller and Harris, 1985;

Dayan, 1986; Harris and Kahl, 1990; Harris, 1992; Comrie, 1994; Merrill, 1994; Harris and Kahl, 1994; Harris and Oltmans, 1997). An ensemble of individual trajectories over a long time period is usually required to construct a meaningful climatology for a site. For example, Bryson (1966) used ten years of twice-daily trajectories for July to identify the source of summertime air masses for Canada. Given the early date of Bryson's study, the trajectory calculations and map generation in his study were done with limited computer resources. The large amount of data analysis involved in the climatological analyses of trajectories is likely the major reason that few studies similar to Bryson's were conducted prior to the 1970's.

(ii) The ARL trajectory model

Improvements in computer technology in the 1970's coincided with an increased attention to air quality issues. As a consequence, considerable resources were devoted to developing computer-based trajectory models to study the long-range atmospheric transport of pollutants. Much of this work was performed at the Air Resources Laboratories (ARL) of the National Oceanic and Atmospheric Administration (NOAA). The ARL models typically have two sets of algorithms. One set calculates the airflow trajectories and requires a meteorological data set as input. The other set of algorithms, which will not be addressed in this thesis, calculates the dispersion and deposition of pollutants along the path of the trajectory and requires data from an air pollution monitoring

network. These models were originally designed to model atmospheric transport in the range of about 100 kilometers to several thousand kilometers (Pack et al., 1978).

An important distinguishing feature of the different ARL trajectory models is the choice of surface on which airflow is calculated. Isobaric models, which assume air motions occur on surfaces of constant pressure, and iso-height models, which assume air motions occur on surfaces of constant height above either sea-level or ground level, are by far the most widely used trajectory models. For example, the first ARL trajectory model (Heffter et al., 1975) and the subsequent ARL-ATAD (for atmospheric transport and dispersion) model (Heffter, 1981) are iso-height trajectory models. The ARL-ATAD model calculates trajectories from gridded wind fields, whereas the original ARL trajectory model used observed winds from upper-air soundings. Both models were designed to calculate trajectories based on averaged winds in a vertically mixed boundary layer with a typical depth of 1-2 kilometers above the surface of the earth. In other words, these models assumed that the material being transported was moving with the mean motion of the boundary layer. These trajectory models have been used to model the transport of a diverse variety of materials capable of being carried over long distances by atmospheric airflow, including air pollutants (e.g., Ashbaugh et al., 1984; Henmi and Bresch, 1985; Poirot and Wishinski, 1986; Comrie, 1994), and plant diseases (e.g., Davis and Main, 1986). The models have also been used to develop airflow climatologies

for sites, such as Barrow, Alaska, and Mauna Loa Observatory, Hawaii (Miller, 1981a, b).

The GAMBIT (for gridded atmospheric multi-level backward isobaric trajectory) model (Harris, 1982) is an example of an isobaric trajectory model developed at ARL together with the Climate Monitoring and Diagnostics Laboratory (CMDL), also of NOAA. This isobaric model and subsequent versions of it have been used to construct airflow climatologies for sites such as Bermuda (Miller and Harris, 1985), Israel (Dayan, 1986), Mauna Loa Observatory, Hawaii (Harris and Kahl, 1990), and the South Pole (Harris, 1992).

Both the iso-height and isobaric models have the advantage of being computationally inexpensive to implement since they can directly use rawinsonde observations (which are available in terms of pressure and height above sea level). Isobaric and iso-height models will theoretically produce similar trajectories. According to Wallace and Hobbs (1977, p. 362), "surfaces of constant pressure are so flat that the horizontal distribution of wind and temperature are virtually the same on a constant pressure surface as on a nearby constant height surface." However, both surfaces have a significant limitation. That is, these are "artificial" surfaces, and air parcels do not necessarily travel along either an isobaric surface or an iso-height surface. Important vertical motions of air parcels are not considered in iso-height and isobaric models.

Isentropic models, on the other hand, assume that air motions are dry adiabatic. In other words, these models assume that potential temperature is conserved along the trajectory and, therefore, the appropriate surfaces for calculating trajectories are surfaces of constant potential temperature. Potential temperature is defined in Wallace and Hobbs (1977; p. 68) as "the temperature which the parcel of air would have if it were expanded or compressed adiabatically from its existing pressure and temperature to a standard pressure". Figure 6 is an example of an isentropic surface at 310 K showing the three-

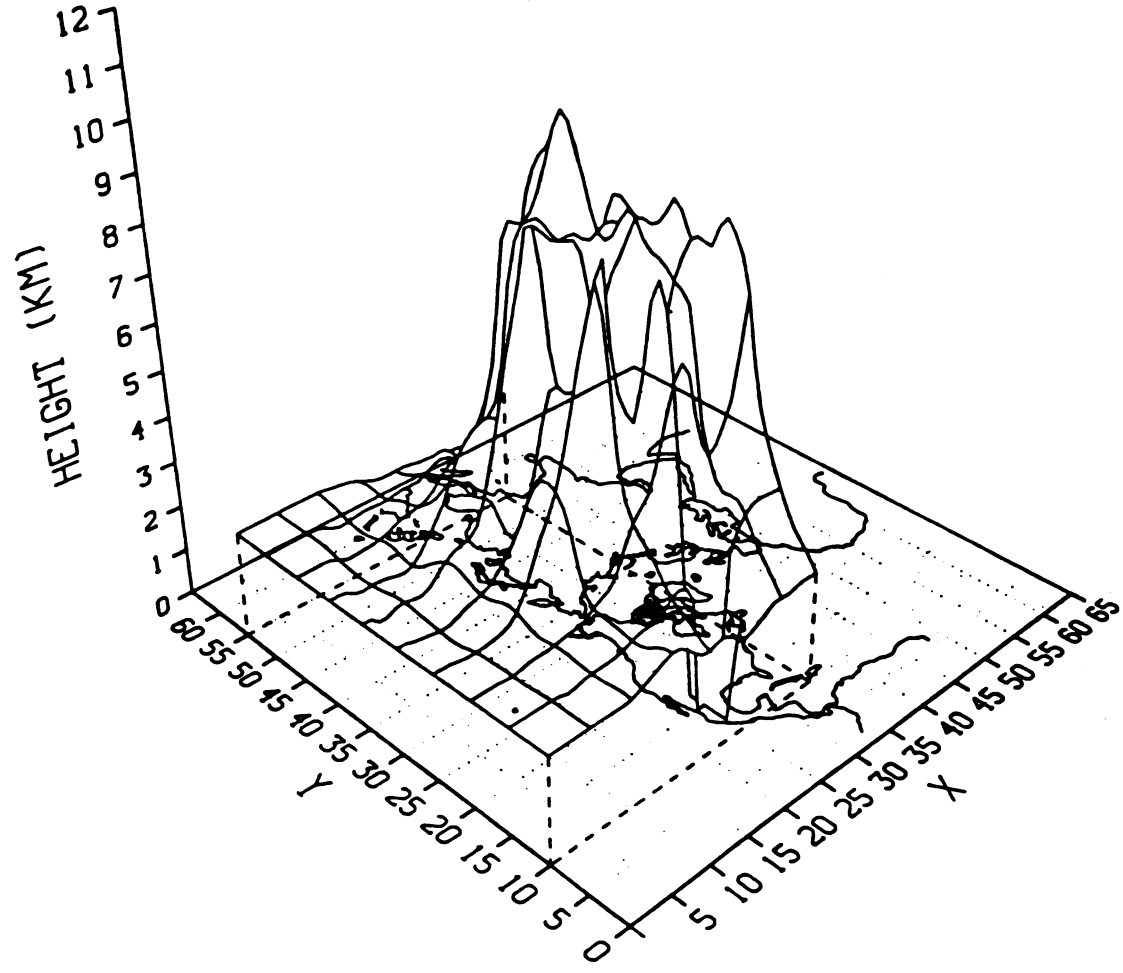

Figure 6. An example of the 310 K isentropic surface.

dimensional relief of this surface of constant potential temperature. Because vertical motions are considered in isentropic models, the assumption of air parcels being transported along surfaces of constant potential temperature is more realistic.

Artz et al. (1985) compared trajectories produced by an isentropic model to trajectories produced by the ARL-ATAD (iso-height) model under a variety of meteorological conditions in both winter and summer, as well as for various heights in the atmosphere. They found that in the absence of fronts, iso-height and isentropic trajectories terminating in the boundary layer "agreed well". However, iso-height trajectories did not agree well with isentropic trajectories near frontal boundaries. In these regions, the isentropic surfaces have considerable topography as they bend upwards or downwards in the atmosphere. Therefore, constant height trajectories may be seriously misleading in these situations. Agreement between the trajectories for the two surfaces is also dependent on wind speed. Light winds cause isentropic and iso-height trajectories to disagree, irrespective of season and height of trajectory, whereas near regions of strong meridional flow and/or large wind gradient where the conditions are baroclinic, isentropic trajectories were "substantially more reliable" (pp. 61-62). On the other hand, in barotropic conditions with strong, steady zonal winds, iso-height and isentropic trajectories were always in "rough agreement".

A disadvantage of isentropic surfaces is that they may intersect the Earth's surface or lose their spatial continuity within the near-surface boundary layer due to diurnal heating and cooling, resulting in erroneous trajectories (Danielsen, 1961; Moore, 1988; Harris and Kahl, 1994). Another disadvantage of isentropic surfaces is that they do not take into account condensation when airflow is along equivalent potential temperature surfaces rather than potential temperature surfaces. Calculating airflow on isentropic surfaces is also more computationally intense compared to calculating airflow along isobaric and iso-height surfaces, making isentropic models almost prohibitive to use for climatological studies until fairly recently.

The previous research cited above suggests that there is no single trajectory model (and vertical coordinate system) that is superior under all types of meteorological conditions. To compensate for this, more complex trajectory models that utilize more than one vertical coordinate system have recently been developed. For example, the ARL HY-SPLIT (for hybrid single-particle Lagrangian integrated trajectory) model (Draxler, 1992) can be used for calculating trajectories on surfaces of constant height, constant pressure, constant potential temperature, as well as several other types of surfaces. The model has been designed to run directly from the ARL site on the World Wide Web (Air Resources Laboratories, 1997), or downloaded from this site via the Internet and executed on a personal computer. As another example, CMDL has developed and utilized for the past several years an isentropic trajectory model

which has the ability to change to layer-averaged (iso-height) mode in the lower boundary layer where isentropic surfaces may lose their continuity (Harris and Kahl, 1994).

(iii) Climatological applications of trajectory models

A number of studies have employed trajectory analysis in climatological research. The first studies to use an ARL trajectory model for a climatological purpose are those of Miller (1981a,b), who used the original ARL model to calculate iso-height trajectories for Barrow, Alaska and Mauna Loa Observatory, Hawaii. The objective of the analysis for Barrow was to better understand the paths and source regions of air parcels contributing to "Arctic haze". For Mauna Loa Observatory, the purpose was to investigate the feasibility of using trajectory analysis to interpret the changing levels of parameters such as trace gases and aerosols that were routinely measured at this site. At both locations, trajectories were calculated twice-daily for five years (1975-1980). At Barrow, 5-day back trajectories were calculated from the mean wind in the 300-2000 meter layer, whereas at Mauna Loa Observatory 10-day back trajectories were calculated for the 3000-5000 meter layer. The trajectories were then categorized by length and direction. This was accomplished by creating a map with three concentric circles of radii between 1000-2000 km with the study site (i.e., Barrow or Mauna Loa Observatory) at the center. Eight spokes were drawn outwards from the center, thereby dividing the mapped area into 24 sectors. Miller found that long

range transport (i.e., trajectories with path lengths greater than 2000 km) was more frequent at Barrow in February and August and that most of these longer trajectories originated from either the north or the south. At Mauna Loa Observatory, over 70% of all trajectories were classified as "long range". In winter, long range trajectories generally originated from the west, whereas in summer most originated from the east.

The GAMBIT trajectory model was used by Miller and Harris (1985) in a similar study concerning airflow climatology based on transport sectors, this time for Bermuda. In their study, the isobaric trajectory model was used to calculate twice-daily 10-day back trajectories for a seven year period (1975-1981) on the 850 mb and 700 mb constant pressure surfaces, instead of for a mixed layer. The 850 mb level was chosen for determining the Bermuda airflow climatology, while the 700 mb level was used as a comparison. However, they found that both levels showed the same kinds of flow patterns. The authors concluded that westerly flow off the North American mainland occurred almost 60% of the time during this period. They also found that precipitation occurred predominantly with southerly trajectories.

Dayan (1986) used the GAMBIT model to compile a five-year (1978-82) climatology of 5-day isobaric back trajectories for Israel. This application differed from that of the previous authors in that Dayan's objective "was to establish a trajectory climatology for the east Mediterranean basin, based on classification of synoptic types, rather than an arbitrary selection of transport sectors" (p.595).

Dayan argued that the 850 mb level was the most representative of the transport layer for human-released pollutants, although specific pollution sources were not addressed. The 850 mb back trajectories were identified for limited direction categories (i.e., WNW, NNW, SE, SW, SSW), which were originally chosen based on frequently occurring synoptic types. He found that approximately two-thirds of the trajectories originated from the WNW and NNW categories. Trajectories from the WNW were slightly more frequent during winter and had the longest fetch over the Mediterranean Sea, whereas those from the NNW were slightly more frequent in the summer and had a shorter fetch.

Several climatological studies have used a multivariate statistical technique known as cluster analysis to summarize large (five- to ten-year) airflow trajectory data sets. Using the GAMBIT model, isobaric trajectory data sets were calculated for Mauna Loa Observatory, Hawaii by Harris and Kahl (1990), and for the South Pole by Harris (1992). In both studies, cluster analysis was used to group (or cluster) similar trajectories in terms of wind speed and wind direction. The airflow climatologies for the two sites were then based on the mean trajectories for each of the clusters by month and by year. This same technique was later used by Harris and Kahl (1994) for Barrow, Alaska and by Harris and Oltmans (1997) for American Samoa. In the latter two studies, however, the CMDL isentropic trajectory model was used to calculate the airflow trajectory data sets.

An important extension of the use of trajectory models in climatological

analysis is the study by Ashbaugh et al. (1984) of "residence time analysis" of atmospheric sulfate concentrations affecting Grand Canyon National Park. Ashbaugh et al. recognized that the usual method of visually examining a large number of trajectories often yielded "semi-quantitative information about the origin of pollutants" (p. 1264). They contended that residence time analysis was a way to statistically quantify the source regions of air parcels arriving at a site. Ashbaugh et al. defined residence time analysis as "the summary of time of residence of trajectory nodes in grid cells", accomplished by overlaying a grid on the trajectory domain, and keeping a count of the number of times that trajectory nodes "resided" over each grid square. The resulting frequency distribution of trajectory nodes revealed ridges and peaks, interpreted as pollution pathways and source/receptor regions, when mapped. For each day in 1980, they calculated 72-hour back trajectories using the ARL-ATAD model (an iso-height model) with the Grand Canyon National Park as the trajectory terminus. A 1° latitude by 1° longitude grid was then centered on the western United States, and a grid cell was incremented each time a 6-hour computational trajectory step (i.e. node) fell within the cell. Probability fields for periods of high and low concentrations of fine particle sulfate at the Grand Canyon were compared to reveal likely pathways of polluted air (from the southwest) and "clean" air (from the north). This methodology was later used by Henmi and Bresch (1985) to study source regions of sulfates for Arizona and New Mexico and for North and South Dakota, and by Comrie (1994) to identify source regions of air masses

laden with atmospheric ozone that were affecting the health of Pennsylvania forests.

Poirot and Wishinski (1986) used a modified version of Ashbaugh et al.'s residence time methodology and adjusted for the background central tendency of trajectories. Since all back trajectories share the same terminus, the chances of a "trajectory passing through a specific grid square at a given distance from the trajectory terminus become increasingly greater as the distance to the terminus decreases" (p.1462). Their method for removing the central tendency is "based on the premise that the background probability of a given grid square is inversely proportional to the area of a ring of one grid square width encompassing that grid square and centered about the trajectory terminus" (p.1462). By removing the background central tendency, areas of high probability could then be considered likely sources of airflow (and pollutants) for their study site, as the correction factor allows direct comparison of probabilities at all locations. They then applied the revised residence time methodology to analyze the sources of summertime aerosols in northern Vermont during three summers (1978-1980) and found that southwesterly trajectories coming from the Ohio River Valley and the lower Great Lakes regions (13.6% of the total) were associated with over 50% of the total sulfate exposure during this time period. Conversely, northwesterly trajectories coming from Canada (50% of the total) were associated with only 10% of the total sulfate exposure. More recently, Merrill (1994) applied this revised methodology to analyze ensembles of

isentropic back trajectories in order to identify seasonal variations in airflow for isolated sites in the Atlantic Ocean. He found that the spatial patterns of potential source areas bore a "clear relationship to features of the large-scale atmospheric circulation" (p. 25,888).

Trajectory analysis has not been limited to studies dealing with air pollution. A limited number of examples in agricultural climatology also exist. For example, Carlson et al. (1992) used isobaric trajectory analysis to study the long range atmospheric transport of insects. Because of their small mass, insects can be passively transported by winds over long distances. Carlson et al. focused on a major influx of potato leafhopper in southern Michigan from 28 May to 3 June, 1989. The potato leafhopper overwinters in the southern United States, and is thought to migrate northward during periods of southerly airflow in spring. Twice-daily back trajectories for three constant pressure surfaces (950 mb, 900 mb, and 850 mb) helped reveal ideal transport conditions from the lower Mississippi River Valley.

Davis and Main (1986) investigated the use of trajectory analysis to identify possible source regions for large-scale plant disease epidemics. Their study focused on the tobacco blue mold epidemics in North Carolina during 1980 and in Kentucky during 1981-82. They used the ARL-ATAD model to calculate boundary-layer back trajectories during the time period coinciding with the first occurrence dates of tobacco blue mold. The trajectories helped identify the source regions of the disease (Northern Florida for the North Carolina site;

South-central Texas for the Kentucky site). Forward trajectories were also calculated from the identified source regions in order to show that these types of trajectories can aid in the prediction of the spread of plant diseases.

(iv) Summary

The analysis and depiction of atmospheric airflow patterns is a complex problem. Wind roses, wind vectors, and streamlines are useful tools that have been frequently used to depict average wind conditions. However, trajectory analysis has been demonstrated by numerous authors to be a successful approach for those studies where knowledge of the origin and path of airflow is essential. The development of computer programs capable of efficiently calculating the required large numbers of trajectories has helped make trajectory analysis attractive for climatological analysis. The majority of these trajectory models were first developed for the study of long-range atmospheric air pollution transport, but they increasingly have been applied to a broader range of research problems.

b. Previous climatological analyses of North American air masses

There are only a few studies that have attempted to construct air mass climatologies for North America or for regions within North America. These studies can generally be placed into two categories, and the following literature review will be organized accordingly. In the first subsection of this review,

climatological studies that classified air masses primarily by temperature and moisture criteria are described. In the second subsection, studies that have based their air mass climatologies on airflow methods, such as streamlines or trajectories, are discussed. Finally, in the third subsection, a summary of the air mass types that have been identified by previous authors for northwest Ohio, irrespective of the methodology employed, is presented.

1) TEMPERATURE- AND MOISTURE-BASED AIR MASS CLASSIFICATIONS

The early air mass studies were not climatologies, but rather were aimed at the development of air mass classification schemes. These schemes classified air mass types in a subjective process based on analyst skill, often using average conditions of temperature and moisture as a guide (Schwartz, 1991; p. 78). Up until the 1950's, when modern upper air data and numerical models came into widespread use, these air mass classification schemes were used as an aid to forecasters (Schwartz, 1991).

As mentioned at the beginning of this chapter, the concept of air masses and their role in the climatology of the middle latitudes was first developed in the early part of this century by V. Bjerknes, J. Bjerknes and T. Bergeron and their collaborators in Europe. They developed the common air mass types and naming conventions still in use today. The air mass names typically identify the characteristics of the source region of the air mass (for example, maritime tropical (mT), and continental polar (cP)).

One of the first of these types of air mass classification schemes for North America was developed by Willett (1933), who attempted to modify the Bjerknes and Bergeron classification. Willett's study was limited to winter and summer. He developed his air mass types based on subjective analysis of twice-daily surface synoptic maps from the U.S. Weather Bureau for North America for the time period of December 1929-March 1930 and July-August 1930. The weather charts were supplemented by upper air observations of temperature and moisture from nine pilot balloon sites scattered about the United States. Willett tabulated mean values of temperature, specific humidity, relative humidity, and equivalent potential temperature at the ground and from ascents at various levels above sea level for the "typical" air mass types at each station. The air mass types he defined for North America included: polar continental (cold and dry), modified polar continental (polar continental air mass becoming warmer and/or more moist), polar Pacific (cold and moist), modified polar Pacific (polar Pacific air mass becoming warmer and drier), polar Atlantic (cold and moist), modified polar Atlantic (polar Atlantic air mass becoming warmer and/or drier), tropical continental (warm and dry), tropical Gulf of Mexico, tropical mid-Atlantic, tropical mid-Pacific (warm and moist), modified tropical moist (tropical maritime air mass becoming colder and/or drier), and tropical subsidence (warm dry subsiding air mass, similar to tropical continental).

Showalter (1939) compared Willett's classification, which he referred to as an "absolute classification", to Bergeron's (1930) "differential classification" and

concluded that the differential classification was more appropriate. Analyzing upper air data from 1935-1936 for all seasons, he defined slightly fewer air mass types than Willett based on mean values of such parameters as specific humidity, relative humidity, air temperature, equivalent potential temperature, and potential temperature, as well as frequency distributions of equivalent potential temperature. The air mass types which Showalter identified as having "practical significance" to the United States in summer were: modified polar (the predominant air mass of summer, consisting of air of polar origin which may be a mixture of continental and maritime, rapidly changing over the continental U.S.), modified polar moist (any polar air mass that is assuming tropical maritime characteristics), modified polar subsidence (cool and dry subsiding air mass), tropical moist (warm and moist, Pacific or Atlantic origin), and superior (dry, subsiding air masses, when the origin is tropical it is equivalent to Willett's category termed "tropical continental" and "tropical subsidence"). For the rest of the year, the following air mass types were thought to be significant: continental polar, modified continental polar, polar Atlantic, polar Pacific, modified polar Pacific, polar moist, modified polar moist, modified polar subsidence, tropical moist, and superior. Showalter also concluded that any classification is only a compromise as to number of types, and that no purpose is served by increasing the number of types (p. 212).

The following authors constructed air mass climatologies for North America and regions within North America using a mixture of subjective and

objective techniques. Brunnschweiler (1952) attempted to develop a "new solution to the problem of climatic classification" using air masses (p. 42). From subjective analysis of daily synoptic maps, the daily outlines of air mass boundaries for North America in the winter months (December, January, February) and summer months (June, July, August) in the years of 1945-1949, were plotted on maps. From these maps, two maps (one for each season) were prepared which depicted "the distribution and tendencies of expansion of the various air masses" (p. 42). He did this by identifying three zones of "prevalence" for the air mass types. These zones included the source region of an air mass (i.e., the region dominated by an air mass at least 80% of the time), the region where an air mass occurred from 20-80% of the time (known as a conflict region if two or more air masses occurred), and the region where an air mass occurred less than 20% of the time. Compared to the previous authors, Brunnschweiler's air mass classifications were much simplified. The air mass types recognized by Brunnschweiler for winter were continental Arctic, continental polar, maritime polar, and maritime tropical. He found there was "a distinctive dominance of Arctic and polar air masses" over North America in winter (p. 48). In summer, the air mass types included continental polar, maritime polar, maritime tropical, and continental tropical. Brunnschweiler found "a less uniform air mass regime" in summer than for winter (p. 48).

Bryson (1966) attempted to describe the influence of summertime air mass dominance on the spatial distribution of the major biotic regions of North

America, especially the boreal forest of Canada. He employed three methods to identify air mass types. The first method was based on temperature, whereas the other two methods were based on airflow and are discussed in the next section. For his first method, Bryson determined the frequency distributions of July daily maximum surface temperature at 120 stations in Canada and the United States for 10 years. This method is an objective technique which assumes that frequency curves, such as surface temperature frequency distributions, are comprised of a series of normal curves. These normal curves, or component normal distributions, can be separated by selecting "the most prominent peaks" from the frequency curve. Bryson contended that the component normal distributions represent different air mass types within the distribution. By decomposing the surface temperature frequency distributions in this manner, Bryson identified ten source regions for summertime air masses. These included 1) the southwest U.S. and Mexico which is a source region for continental tropical air masses, 2) the Gulf of Mexico which is a source region for maritime tropical air masses, 3) Montana and Wyoming which is a source region for a mild, dry air mass termed by Bryson "Northern Rockies Pacific", 4) the Liard River gap of the cordillera in the Yukon Territory which is a source region for what Bryson termed "Yukon Pacific" air masses, 5) the Mackenzie Valley region of Alaska, a source region of "Alaskan" air masses, 6) the Canadian Arctic archipelago, a source region for cold air masses, which were termed "Eastern Arctic", 7) the Arctic Ocean whose cold air masses were

termed "Western Arctic", 8) the Hudson Bay area, a source of cold, dry air masses with long residence time, termed "Hudson Bay", 9) the Atlantic Ocean, entering Canada from Labrador, a source of maritime air masses termed "Atlantic", 10) the Canadian Rockies in Alberta, a source of mild, dry air masses termed "Canadian Rockies Pacific". When related to the boreal forest in Canada, Arctic air masses were found to occupy the area north of the tree line more than half the days during July, while mild Pacific (i.e., Northern Rockies Pacific and Canadian Rockies Pacific) air masses occupied the region directly south more than half the days.

The air mass climatology for the North Central United States presented in Schwartz (1982) and Schwartz et al. (1985) was developed using an air mass classification technique based on quantitative temperature and moisture limits for a set of air mass types specific to this region. Air mass categories were drawn from conventional nomenclature and included six discrete types: continental, Pacific, tropical, dilute tropical, dry tropical, and polar (summer only). The polar air mass type, similar to Showalter's (1939) "modified polar" air mass type of summer, is a combination of continental and Pacific air mass types thought to be indistinguishable from one another during summer. The temperature and moisture limits for each air mass type were developed by following air masses of known origin on sequential weather maps. These limits were applied to ten years (1970-1979) of daily 1200 UTC 850 mb temperature and surface dewpoint temperature observations in January (for winter), April (for spring), July (for

summer), and October (for autumn) from a scattering of weather stations in the North Central United States. The limits were subjectively adjusted for location within the study area and for season. Temperature and moisture observations not falling within the limits of any air mass type were classified as "transitional" and, according to Schwartz and Schwartz et al., probably represented a mixture of air mass types. From the resulting air mass climatology of the North Central United States, Schwartz and Schwartz et al. concluded that:

1) continental air masses dominated the northern portion of the study area in all seasons and were also "influential" elsewhere in the study area; 2) Pacific air masses were "prominent" in the western portion of the study area, particularly in spring and autumn, "but of less importance elsewhere"; 3) dilute tropical and tropical air masses were "important" in the southern and eastern portions; 4) dry tropical air masses were "a summer season phenomenon affecting mainly the western portions of the study area"; and 5) transitional conditions "accounted for about 20-30% of the total days at a station in any season."

Further building on the research of Schwartz (1982) and Schwartz et al. (1985), Schwartz (1991) used component normal distributions, as in Bryson (1966) (described above), to deconstruct the frequency curves of daily (1200 UTC) 850 mb temperature and dewpoint values to identify the same air mass types as the two earlier studies. As in Schwartz (1982) and Schwartz et al. (1985), data were analyzed for January, April, July, and October for the same stations in the North Central United States, although using a longer time period

(1958-1981). The component normal distribution data were then merged with the previously defined numerical limits of air mass types from Schwartz (1982) and Schwartz et al. (1985), yielding revised limits with (assumed) greater numerical precision. The spatial distributions of seasonal air mass frequencies in the North Central United States resulting from this approach were very similar to the those from Schwartz (1982) and Schwartz et al. (1985). In a subsequent study, Schwartz and Skeeter (1994) sought to relate mid-tropospheric flow patterns to the temperature- and moisture-based air mass frequency patterns constructed in Schwartz (1982), Schwartz et al. (1985) and Schwartz (1991). They concluded that spatial distribution of air mass frequency patterns could be "quantitatively related to a small number of meaningful 500 mb height and surface pressure patterns in all seasons" (p. 462). Schwartz (1995) investigated trends in the air mass frequency distributions from Schwartz (1991) and Schwartz and Skeeter (1994) in order to assess regional climate change during the 1958-1992 time period. His results suggested that there was an increased frequency of tropical air masses in the North Central United States in spring and summer during the 1958-1992 time period. A decrease in the frequency of polar air masses also occurred in summer, as well as a warming of the dry tropical air masses. In winter, continental air masses showed "evidence of warming", while in autumn there were "no major air mass characteristic trends".

2) AIRFLOW BASED AIR MASS CLIMATOLOGIES

An early example of the use of streamline analysis in climatological research is Borchert's (1950) attempt to explain the location and shape of the grasslands region of North America in terms of climatic controls. Borchert's contention was that streamlines of the resultant wind would indicate the paths of the major air masses affecting the region. The resultant wind of the 500 meter level was calculated at approximately 100 sites east of the Rocky Mountains from 14 years of pilot balloon observations, and streamlines were then subjectively drawn. The 500 meter level was chosen because of its situation far enough above the surface to eliminate most frictional effects, yet low enough to obtain accurate and regular pilot balloon observations. Borchert visually inspected the streamline plots and inferred the presence (in all months) of three mean air streams east of the Rockies from three distinct source regions. The source regions were, 1) the sub-tropical Atlantic anticyclone, 2) the Arctic region, and 3) the eastern base of the Rockies. The airstream that moved westerly from the eastern base of the Rockies dominated the grasslands in winter. The Pacific air masses in this stream descended the Rockies, losing their moisture, resulting in low precipitation over the grasslands compared to the bordering regions to the north and south. Borchert attributed the characteristic wedge shape of the grasslands region to it's location in this belt of strong westerly flow in winter. Along the northern border of the grasslands, the Pacific airstream, according to Borchert, undergoes "cyclonic convergence ... where it is led into the Alberta

storm path" (p. 22), resulting in increased snowfall on the northern border of the region. The area north of the grasslands was dominated by airflow from the Arctic, while the area to the southeast of the grasslands was dominated by anticyclonic flow of moisture-laden tropical air, resulting in a larger amount of precipitation in this area. Streamlines indicated that this flow of tropical air "penetrates farther into the continent in summer", pinching out the Pacific airstream at about the 100th meridian (p. 23).

In a unique and comprehensive study, Bryson (1966) used both streamline analysis and trajectory analysis to supplement a temperature-based air mass classification scheme (described in the previous section). As mentioned earlier, the focus of Bryson's study was to investigate the role of air mass dominance on the spatial distribution of the major biotic regions in North America, particularly Canada. In the streamline approach, mean resultant surface wind measured at weather stations east of the Rockies in North America for each month during the period 1930-1945, were used to construct monthly streamline maps. Bryson contended that mean confluence zones represented fronts separating air masses originating from different source regions. Besides the confluence evident in both summer and winter between the air masses originating from the Arctic and Pacific source regions, a second major confluence zone stretched from Colorado to Maine. This confluence zone was present during much of the year, although it was hypothesized that the types of air masses separated by the confluence zone varied by season. The confluence

zone appeared to separate mild Pacific air from "return polar" air (i.e., modified continental polar or maritime polar air, returning northward within a stagnant anticyclone) in November through May. During the remaining months of the year, the confluence zone separated maritime tropical air masses from Arctic air masses. He observed that the cornbelt of the midwest United States was situated in a region that was dominated by Pacific air masses in winter and maritime tropical air masses in summer.

Bryson's trajectory analysis supported the contention that the tundra-boreal forest boundary occurs where air masses originating from the Pacific Ocean and the Arctic are equally frequent. A 5° latitude and longitude grid overlay was centered on Canada, and trajectories were calculated for the grid intersections. All trajectories were calculated using the geostrophic, rather than the actual, wind from surface synoptic charts. The analysis was based on 10 years (1945-1951 and 1954-1956) of twice-daily observations for July. For each grid intersection, the trajectories were grouped into four categories (considered to be air mass source regions) according to their point of origin, and the frequency of trajectories in each category was determined. The categories (i.e., source regions) were Arctic, Pacific, Atlantic, and the United States. Isopleth maps of the frequency of air masses from the different source regions indicated that the most important source regions for Canada in July were the Arctic and the Pacific Ocean. Air masses originating from the Arctic source region were most important in northern and eastern parts of Canada, while air masses

originating from the Pacific Ocean were most important in the western parts of Canada, particularly west of the Rocky Mountains. Bryson found that the transition zone, where air masses originating from the Arctic and Pacific Ocean source regions were equally frequent, coincided with the tundra-boreal forest border.

In a broader study, Wendland and Bryson (1981) used streamline analysis to "show the characteristics of some air masses, and discuss how changes in location of mean confluences influence changing weather patterns or climate" in the Northern Hemisphere (p. 256). Again, they assumed that confluence zones represented fronts separating air masses, while divergent flow indicated air mass source regions. Following the procedure of Bryson (1966), streamlines were constructed from monthly resultant winds, although a longer period of record (1943-1963) and a finer grid mesh (3° latitude) were used compared to Bryson's (1966) earlier study. The streamline analyses suggested nineteen source regions of air masses throughout the year affecting the Northern Hemisphere. The source regions which affected North America were found to be the North Pacific Ocean, North Atlantic Ocean, and Arctic (all are important throughout the year); Klondike (important in winter); the Ohio Valley (important in autumn); and the High Plains (important in winter). Wendland and Bryson found that oceanic source regions, such as the subtropical Atlantic and Pacific anticyclones, were present in all seasons. Continental source regions, on the other hand, were evident only during various parts of the year.

3) SUMMARY OF AIR MASS TYPES FOUND IN PREVIOUS STUDIES FOR NORTHWEST OHIO.

In the following subsection, the results of the studies discussed above, as applied to northwest Ohio, are summarized. The frequency, type, and origin of different air masses were interpolated from the maps, graphs, and tables presented in the original papers. The different methods and definitions employed by the authors make direct comparison of the results from these studies difficult. However, an attempt is made to identify, as much as possible, the general patterns for each season.

(i) Winter

There is no general consensus among the previous authors regarding the type of air masses that influence northwest Ohio during winter. Brunnschweiler (1952), Schwartz (1982; 1991), and Schwartz et al. (1985) all found a dominance of continental sources affecting northwest Ohio in winter. Schwartz (1982; 1991) and Schwartz et al. (1985) found that approximately 70% of all air masses affecting northwest Ohio during January (considered representative of winter) were from continental sources (Table 1). Air masses originating from the Pacific Ocean were present on 8-13% of all January days, tropical air masses originating from the Gulf of Mexico were present 2-7% of the time, and "transitional" conditions (thought to be a mixture of different air masses) were present from 14-15% of the time. Brunnschweiler (1952) found continental polar air masses occurred 80% of the time over northwest Ohio in the winter months of

December, January and February. It is not possible from his paper to discern which air masses occurred in northwest Ohio during the remaining 20% of the time. On the other hand, Borchert's (1950) streamline analysis suggests that during winter northwest Ohio lies in a belt of westerly or west-southwesterly airflow, presumably transporting modified Pacific air into northwest Ohio. His results are confused, however, by the location of a confluence zone running nearly horizontally through northwest Ohio. Also, the axis of maximum cyclone frequency in winter, identified from historical weather maps, passes through northwest Ohio. These latter two features suggest that air masses from the Pacific, the interior of Canada, and the Gulf of Mexico may be equally important during winter in this region.

Bryson's (1966) results are in better agreement with Borchert's analyses than with Brunnschweiler's and Schwartz's results, in that they, too, suggest the equal importance of Pacific and polar air masses. His streamline analysis also pointed to a confluence zone over northwest Ohio, which Bryson interpreted as the mean location of the front separating Pacific from "return polar" air masses. Wendland and Bryson's (1981) results further add confusion. The nearby southern Ohio Valley and the High Plains appear to be the most important source regions of wintertime air masses, especially in early winter (i.e. December and January). These results agree well with Borchert's (1950) and Bryson's (1966) identification of airflow which is primarily west-southwesterly for northwest Ohio during winter. The role of continental polar air masses, identified as

Table 1.

Air mass frequencies (%) for northwest Ohio *

	Cont/Polar	Pacific	Dilute Trop.	Trop.	Dry Trop.	Unclassed	Total
Winter	69.2 (68.8)**	12.8 (8.1)	2.4 (6.7)	0.2 (2.4)	-	15.4 (14.0)	84.6 (86.0)
Spring	36.7 (50.1)	30.4 (13.7)	10.9 (9.9)	2.5 (9.1)	-	19.5 (17.2)	80.5 (82.8)
Summer	43.9 (42.3)	-	-	27.0 (30.3)	0.9 (2.2)	28.2 (25.2)	71.8 (74.8)
Autumn	31.6 (33.1)	29.4 (22.5)	17.1 (13.0)	1.2 (4.5)	-	20.7 (26.9)	79.3 (73.1)

** Air mass frequencies for northwest Ohio were derived by averaging the air mass frequencies provided by the authors for Flint MI and Dayton OH in Schwartz (1982), Schwartz et al. (1985) and Schwartz (1991).*

*** Numbers not in parentheses were derived from Schwartz (1982) and Schwartz et al. (1985); numbers in parentheses were derived from Schwartz (1991).*

important by Brunnschweiler (1952) and Schwartz (1982) is unclear from Wendland and Bryson's results.

(ii) Spring

Schwartz's (1982) and Schwartz et al.'s (1985) results suggest that in April (taken as representative of spring) the frequency of continental air masses decreases dramatically (Table 1.). This decrease is accompanied by increases in the frequency of Pacific and dilute tropical air masses. On the other hand, only a moderate drop in the frequency of continental air masses is indicated in Schwartz's (1991) later study. Pacific air masses were also not found to occur as frequently as the earlier studies. However, tropical air masses were found more frequently by Schwartz (1991) than by Schwartz (1982) and Schwartz et al. (1985). Again, Bryson's (1966) streamline analysis results are not in complete agreement. His results suggest that, although Pacific and "return polar" air masses are approximately equally frequent in March, Arctic air masses (often originating over Hudson Bay) and maritime tropical air masses are dominant in northwest Ohio during April and May. Both Bryson's and Borchert's (1950) analyses suggest that as spring progresses the confluence zone originally lying over northwest Ohio shifts northward. As a result, southwesterly airflow, capable of transporting maritime tropical air masses, is evident over northwest Ohio. Wendland and Bryson's (1981) results also indicate maritime tropical air masses to be important in spring and found that northwest Ohio is located close to a confluence zone of Arctic and subtropical North Atlantic air streams originating

just east of Florida. Brunnschweiler (1952) did not analyze springtime air mass frequencies.

(iii) Summer

Both Bryson's (1966), Wendland and Bryson's (1981), and Borchert's (1950) streamline analyses suggest that northwest Ohio is primarily influenced by maritime tropical air during summer originating from the Gulf of Mexico or from the Caribbean Sea. Bryson's and Borchert's analyses both indicate that the mean confluence zone is now located well north of northwest Ohio. On the other hand, Bryson's temperature analysis (Table 2) results suggest that air masses of Pacific origin are more important than tropical air masses. In contrast, Brunnschweiler's (1952) and Wendland and Bryson's (1981) analyses do not

Table 2.

Air mass frequency in northwest Ohio (July)*

continental Tropical	5%
maritime Tropical	30%
mild Pacific	50%
cool Pacific	<10%
Arctic	<10%

** Air mass frequencies are based on temperature analyses using component normal distributions from Bryson(1966).*

suggest that Pacific air is important at all. Rather, Wendland and Bryson found the nearby Ohio Valley to be a frequent source of summertime air masses for

northwest Ohio. Brunnschweiler's (1952) results show northwest Ohio to be in a "conflict region" of continental Polar and maritime tropical air masses.

Brunnschweiler defined a conflict region as an area where two or more air masses each occur between 20-80% of the time in the region. Schwartz (1982, 1991) and Schwartz et al. (1985) combined their continental and Pacific air mass types for summer and found that this combined type was relatively frequent (42-44%). However, it is not possible to distinguish from the results which of the two source regions is most influential. Their results also suggest that tropical air masses and transitional conditions are equally important in northwest Ohio in summer, each occurring on average from 25-30% of all days.

(iv) Autumn

The results of several of the previous climatological studies suggest that autumn is truly a transitional season. For example, Schwartz (1982; 1991) and Schwartz et al. (1985) found that continental, Pacific, dilute tropical, and transitional air masses are all common during autumn (Table 1). Bryson (1966) found that in early autumn, as in summer, the mean confluence zone was located north of northwest Ohio and, consequently, tropical air masses from the Gulf of Mexico were dominant. However, in late autumn the confluence zone once again became situated over northwest Ohio. This confluence zone separated Pacific air from "return polar" air, similar to what was earlier identified for winter. In contrast to the other studies, Wendland and Bryson (1981) found

that the primary air mass source region during autumn is the nearby Ohio Valley. Brunnschweiler's (1952) and Borchert's (1950) studies did not encompass the autumn season.

3. Specific Objectives

The literature review presented above indicates that a number of different methodologies have been used to identify air mass types and source regions, and that, at least for northwest Ohio, the type of methodology can have a large influence on the interpretation of the most important air mass source regions for a location and of the seasonal changes in the dominant source regions. However, one methodology that has been infrequently used is that of trajectory analysis. Conceptually, trajectory analysis is a more appropriate technique for preparing an air mass climatology, since air masses can actually be traced back to their general region of origin. Furthermore, it is possible using trajectory analysis to make inferences about the modifications of air masses along the trajectory that is not possible with other methodologies. The main objective of this thesis is to use trajectory analysis to prepare an air mass climatology for northwest Ohio and to compare the resulting climatology to those prepared using alternative methodologies.

In order to accomplish this objective new techniques for displaying and interpreting trajectories are required, since current trajectory display and analysis software produces maps which are difficult and cumbersome to interpret,

especially when the number of trajectories is large. Thus, an additional objective of this thesis is to explore and develop visualization and display software appropriate for the analysis of an ensemble of trajectories. Because of the large number of trajectories that are required for climatological analysis, these techniques must be computer based, and, since personal computers are more and more ubiquitous and powerful, the personal computer platform was chosen. The approach employed is a raster geographic information system (GIS)-based technique, described in subsequent chapters. The development and implementation of the GIS-based methods for the display and analysis of a large ensemble of airflow trajectories are instrumental to the main objective of this research effort.

This research will hopefully improve our understanding of the air mass climatology of northwest Ohio, and will also provide potentially useful tools for constructing general purpose airflow climatologies, beneficial in a broad range of disciplines such as entomology, pathology, and atmospheric chemistry.

4. Organization of the thesis

The thesis is organized as follows. The next chapter (Chapter II, entitled *Data and Trajectory Calculation*, describes the choice of study location, the meteorological data set from which the trajectories were calculated, and the method used to calculate the individual trajectories. Chapter III (*GIS Methods*) describes the process of developing the GIS database and applications for

analyzing the spatial distribution of the rasterized trajectory nodes. Chapter IV (*Results and Discussion*) develops an air mass climatology for northwest Ohio. Results of previous air mass studies for the area (summarized in Chapter I) are compared to the results produced by this research effort. Finally, in Chapter V (*Conclusions*) the major conclusions, including recommendations for further study, are provided.

CHAPTER II

DATA AND TRAJECTORY CALCULATION

1. Overview

As stated in Chapter I, the objective of this study is to construct an air mass climatology based on airflow trajectories for a site in northwest Ohio. In this chapter, the atmospheric surface along which the airflow trajectories were calculated, the meteorological data set used to calculate the trajectories, and the algorithm used to determine the trajectories are described. Also, the findings of previous research on the general accuracy of airflow trajectories is summarized. This latter material is provided so that the reader can better interpret the results of the climatological analysis. The geographic information system techniques used to summarize and display the trajectories will be described in the following chapter.

2. Choice of analysis level

A constant pressure (isobaric) trajectory model, rather than a constant height or constant potential temperature (isentropic) model, was used in this study. The primary reason for the choice of this type of model is the availability of historical wind data sets for surfaces of constant pressure. Previous work, cited in Chapter I, also suggests that the choice of vertical coordinate (i.e., isobaric, isentropic, iso-height) does not have a large impact on the accuracy of

trajectories and/or their interpretation.

All trajectory calculations were performed for the 850 mb constant pressure surface. This surface was chosen for several reasons. First, this surface is one of the standard levels for which meteorological observations are routinely reported worldwide. Second, because of its height (approximately 1200-1500 meters above sea-level), the 850 mb surface is not strongly influenced by frictional forces that affect airflow in the boundary layer, thereby making it a reliable choice for representing long-range airflow. Finally, this surface has been widely used in previous climatological research. As noted in the previous chapter, several authors chose the 850 mb constant pressure surface for developing airflow climatologies. Most noteworthy were the seven-year and five-year airflow climatologies by Miller and Harris (1985) and Dayan (1986). Another example is the paper by Winkler et al. (1996) who used gridded observed 850 mb winds to construct a 21-year airflow climatology for the springtime months over central and eastern North America. Also, the 850 mb level was used by Barry (1967), Schwartz (1982; 1991) and Schwartz et al. (1985) to assess air mass type based on temperature and moisture measurements. They chose the 850 mb surface for their analyses, because temperature and moisture parameters at this level are not as affected by the diurnal heating and cooling cycle compared to lower atmospheric surfaces.

3. Wind data set

The original source of the wind data, which serves as input to the trajectory model used in this study, is the National Meteorological Center (NMC) Northern Hemisphere grids (or analyses). The NMC grids used in this study were obtained on CD-ROM from the National Center for Atmospheric Research (NCAR), which keeps an archive of the NMC data. The NMC grids of wind data are produced by integrating hemispheric wind data with a first-guess field from a Numerical Weather Prediction (NWP) model. Hemispheric wind data are obtained from rawinsonde, pilot balloon, and aircraft reports, and from satellite measurements of cloud movement. A limitation of the wind observations is that data coverage over much of the oceans and polar regions is sparse. In an attempt to improve coverage and accuracy over data sparse areas, the observed winds are integrated with a first-guess field. The first-guess analysis is either a 6- or 12-hour forecast from a NWP model using a previous analysis as its initial condition (Trenberth and Olson, 1988).

According to Trenberth and Olson (1988), the major concern with the accuracy of the NMC grids involves changes in the NWP model used to produce the first-guess field. These changes appear to have affected the analyses mainly in the Southern Hemisphere, the tropics, and in specific parameters, such as relative humidity (p. 1048). Comparisons of the NMC grids for 1980-1986 with those obtained from the European Center for Medium-range Weather Forecasts (ECMWF), showed "widespread agreement between the analyses

from the two centers over the NH extratropics" (p. 1055). These results suggest that the potential impact of changes at NMC in the production of first-guess fields on the trajectory climatology presented here for northwest Ohio is likely to be small, as the study site is located in the North Hemisphere extratropics where the models were in agreement.

The resulting data set after the wind observations were integrated with the NWP first-guess field, consists of gridded values of the u (east-west) and v (north-south) wind components for standard pressure levels (1000, 850, 700, and 500 mb). The twice-daily (0000 and 1200 UTC) grids consist of 1977 points over the Northern Hemisphere. The points are equally spaced when viewed on a pole-centered polar-stereographic projection. The grid resolution is 381 kilometers at 60°N (Jenne, 1975).

Unfortunately, some wind fields are missing in the NMC data set. Table 3 summarizes the missing data as percentages in each year, as well as the major periods when data gaps occurred during each year. For this study, linear interpolation was used to replace missing data for isolated 12-hour time periods. When two or more consecutive 12-hour periods were missing interpolation of the missing data did not occur.

Table 3.

Summary of missing 850 mb NMC u and v wind analyses

Year	Missing analyses	Major gaps in the analyses
1976	2/732 (0.3%)	-
1977	8/730 (1.1%)	-
1978	5/730 (0.7%)	-
1979	6/730 (0.8%)	-
1980	35/732 (4.8%)	-
1981	68/730 (9.3%)	2/1 - 2/7, 10/4 - 10/10
1982	82/730 (11.2%)	7/4 - 7/10
1983	101/730 (13.8%)	4/9 - 4/30, 6/18 - 6/21
1984	64/732 (8.7%)	10/28 - 11/2
1985	27/730 (3.7%)	-

4. Study period

The ten year period from January 1, 1976, through December 31, 1985, was used to develop the air mass climatology. The study period was restricted to ten years because it was thought to be sufficient for detecting variability in air mass types. The majority of the previous air mass and airflow climatologies cited in Chapter I were based on five to ten years of observations (Brunnschweiler, 1952; Bryson, 1966; Miller, 1981a; 1981b; Schwartz, 1982; Schwartz et al., 1985; Miller and Harris, 1985; Dayan, 1986; Harris, 1992; Merrill, 1994; Harris and Kahl, 1994; Harris and Oltmans, 1997). The *Climatological Atlas of the United States* (Department of Commerce, 1968) also used ten years as a basis for its wind climatology maps.

5. Calculation of the trajectories

a. Choice of terminus point

Theoretically, trajectories can be calculated for each of the 1977 points of the NMC grid. For this study, however, a grid point in northwest Ohio (more precisely 41.56°N, 84.09°W) serves as the terminus for all the trajectory analyses. As discussed in Chapter 1, the primary reason that northwest Ohio was chosen as the study location is the large variability in air mass types that influence this region. It is also of interest due to the disagreements and uncertainties of the results from previous air mass climatologies for this region.

b. Selection of a subgrid

The NMC hemispheric grids, as their name implies, cover the entire Northern Hemisphere. The first step in the analysis was to extract smaller, more manageable subgrids appropriate for trajectory calculations with northwest Ohio as the terminus. A 19 x 22 gridpoint subgrid, centered approximately on the study location, was selected. The geographic area of the subgrids encompassed the entire area of North America, including most of Mexico and the Caribbean (Figure 7). The determination of the size and coverage of the subgrid area was based on the horizontal data coverage required for 5-day backward trajectories starting from the terminus in northwest Ohio. The subgrid was also chose to include the likely source regions for air masses affecting the study site.

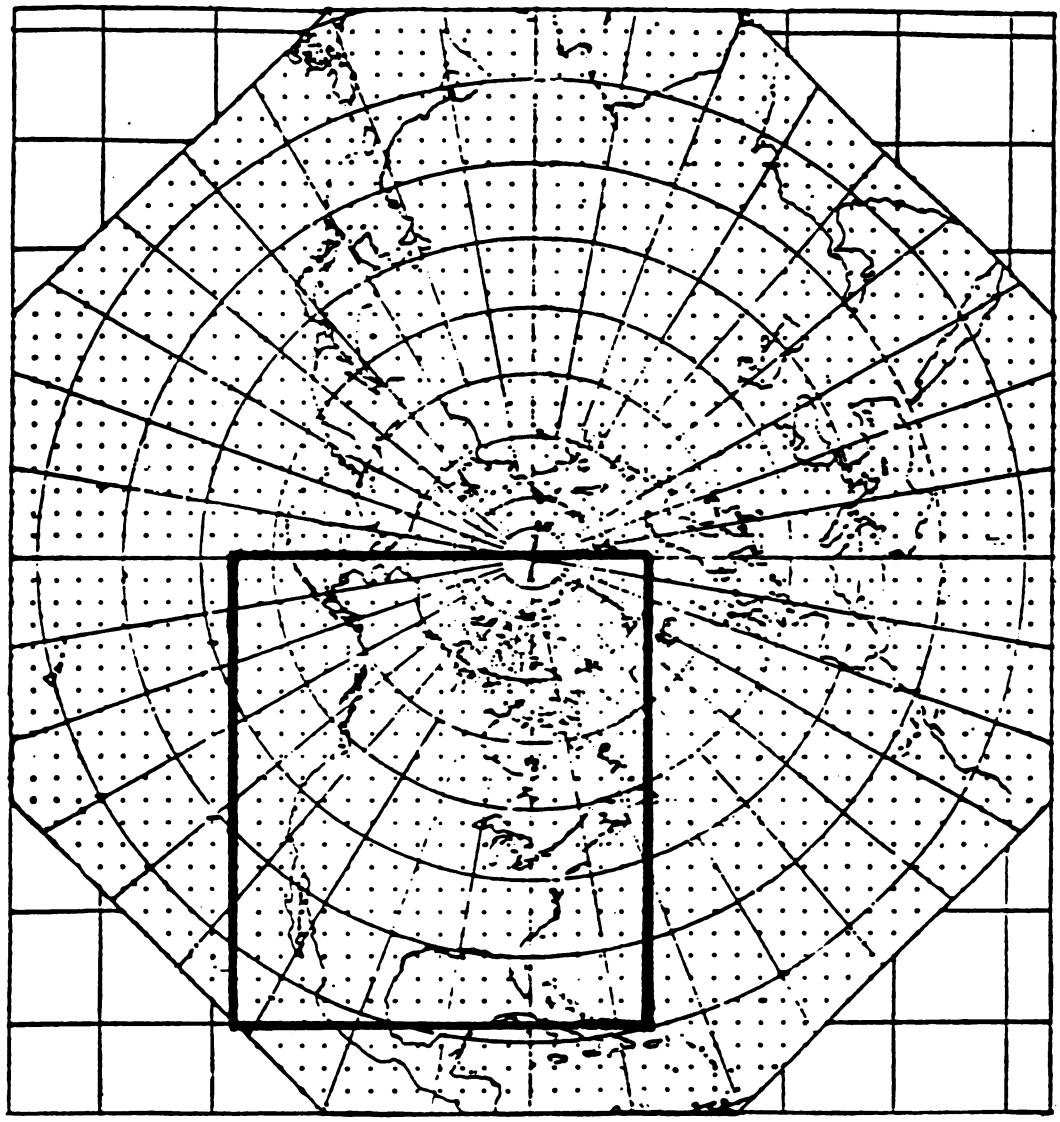

Figure 7. The NMC 47x51 grid (from Jenne (1975), p. 18) with the 19x22 subgrid delineated.

c. Conversion from grid- to compass-oriented u and v wind component

As mentioned earlier, the gridded wind data were available twice daily (0000 and 1200 UTC) at the standard pressure levels in the form of u and v wind components. The equation $\mathbf{V} = u\mathbf{i} + v\mathbf{j}$, where **V** is the horizontal velocity vector, and **i** and **j** are the unit velocity vectors in the u and v directions, defines the u and v horizontal components of the wind (Wallace and Hobbs, 1977, p. 362). The zonal (u) component of the wind is westerly when $\mathbf{i} > 0$, and easterly when $\mathbf{i} < 0$. The meridional (v) component of the wind is southerly when $\mathbf{j} > 0$, and northerly when $\mathbf{j} < 0$. The u and v wind components from the NMC grids were oriented to the grid rather than by compass direction. It was necessary to first convert the wind components to compass direction before calculating the trajectories. This was accomplished by executing a computer program supplied for this purpose by NMC.

d. The trajectory model

The model used to calculate the airflow trajectory data set for this study was adapted from Scott and Achtemeier (1987). This model calculates trajectories backward in time from a site location using a grid of u and v wind components. Their technique was "an adaptation of an accurate objective streamline analysis technique" (p. 1248). The only difference in the algorithm used by Scott and Achtemeier (1987) and the one employed in this study is that their model computed trajectory segments in 3-hour intervals, while 6-hour

intervals were used here. The larger time interval was employed here because of concern about the accuracy of 3-hour points when data are only available twice-daily.

Each trajectory is followed backward in time from the terminus site for five days. Note that 5-day back trajectories were used in several airflow climatologies described in Chapter I (e.g., Miller (1981a, b), Dayan (1986), Harris (1992)). A 5-day trajectory consists of 20 individually-computed 6-hour segments placed end to end. The segment endpoints will be referred to here as "nodes" and are identified by latitude, longitude coordinates. The spatial distance between 6-hour nodes in a trajectory is a function of the strength (or speed) of the wind. That is, weak winds will yield shorter trajectories than stronger winds. When missing data values were encountered, the trajectory calculation was terminated.

Each 6-hour back trajectory segment was calculated by interpolating in time between two consecutive data files (between 0000 and 1200 UTC or between 1200 and 0000 UTC). The calculation begins with a u, v wind component pair at location 1 (the terminus point) at a particular time (say 1200 UTC) (see Figure 8). First, an initial segment ending at 2' was calculated by:

a) separately multiplying the 1200 UTC u and v wind components (in units of kilometers/hour) at the trajectory terminus by 6 hours, thereby estimating, assuming a steady wind, the distance (DISu

and DISv) traveled by an air parcel during the 6-hour period in the east-west and north-south directions;

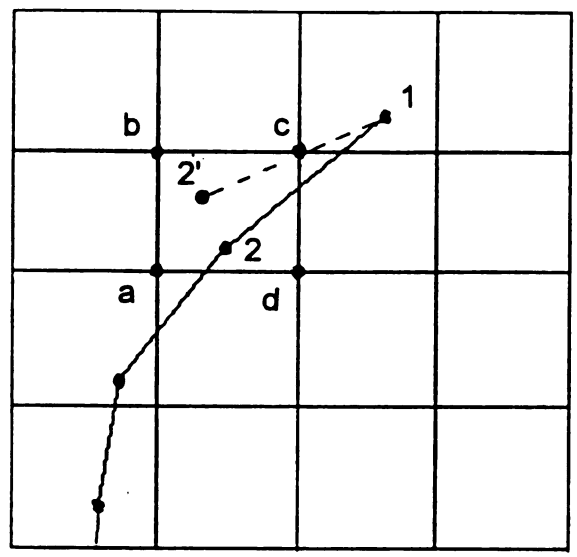

Figure 8. The trajectory calculation

b) determining an initial estimate of latitude and longitude (lati and longi) of the air parcel at 2' by subtracting the distance traveled (DISu and DISv) in the 6 hours in the u and v directions from the latitude and longitude (latt and longt) values at the terminus site and dividing by the number of kilometers per degree of latitude (X) or longitude (Y). X was defined as 111.0 km, the approximate

value for 38°N latitude (Robinson et al., 1978, p. 401). X was assumed to be a constant, given the small change in the length of a degree of latitude with location on the Earth's surface. Y was determined from the cosine of the latitude. The calculations in this analysis step can be summarized as:

lati = latt - DISv / X

longi = longt - DISu / Y, where Y is found from the following:

Y= cosine (lati) * X

The next step was to find the u and v components for the initial point (ui, vi). This is accomplished by first averaging for the grid points that surround the initial point (a, b, c, d on Figure 8), the u, v pairs for 1200 and 0000 UTC. This gives an estimate of the 0600 UTC u, v components for these points. The 0600 UTC wind components for the initial point is then found using a bilinear interpolation of the u, v pairs at the four surrounding gridpoints. These calculations can be summarized as:

ui = ua * (I + 1 - I') * (J + 1 - J') +
ud * (I' - I) * (J + 1 - J') +
ub * (J' - J) * (I + 1 - I') +
uc * (I' - I) * (J' - J)

vi = va * (I + 1 - I') * (J + 1 - J') +
vd * (I' - I) * (J + 1 - J') +
vb * (J' - J) * (I + 1 - I') +
vc * (I - I') * (J' - J)

where I is the grid column coordinate at a; I' is the grid column coordinate at 2'; J is the grid row coordinate at a; and J' is the grid row coordinate at 2'.

Next, to refine the estimate of the air parcel's location 6 hours previously, the original u, v pair from location 1 (i.e., the terminus) at 1200 UTC, and the estimated u, v pair from 2' at 0600 UTC are averaged. The average u, v components are then used to recalculate the trajectory segment using the same methods described above. Point 2 on Figure 8 indicates the refined estimate of the air parcel's location. This whole process is repeated for each subsequent 6-hour segment.

e. Monthly percentages of trajectory nodes by compass quadrant

The objective of this step was to obtain, for each month, a quantitative measure of the directionality of airflow to the terminus. A computer program (written in the Fortran language) was used to compute the ratio (expressed as a percentage) of the number of trajectory nodes in each of the four quadrants (NE, SE, NW, SW) surrounding the terminus to the total number of trajectory nodes for each month. The quadrants were defined by the terminus latitude and longitude coordinate values. For example, trajectory nodes classified as being in the northeast (NE) quadrant were required to have latitude coordinate values greater than the terminus latitude (41.56°N) and longitude coordinate values less than the terminus longitude (84.09°W). To better define where the 5-day back

trajectories originated, the ratio of the number of trajectory nodes at -120 hours (i.e., 5 days previously) in each of the four quadrants to the total number of -120 hour trajectory nodes was also calculated. These data supplement the frequency plot maps of the trajectory nodes presented in Chapter 4.

6. Trajectory accuracy

The accuracy of airflow trajectory models has been the subject of many studies (e.g., Hoecker, 1977; Pack et al., 1978; Clark et al., 1983; Kuo et al., 1985; Scott and Achtemeier, 1987; Kahl and Samson, 1988). Previous studies suggest that trajectory error increases as the scale of meteorological events decreases due to the coarse spatial and temporal resolution of the wind field data. Events such as quickly-moving fronts may not be resolved at these scales. Calculated airflow trajectories, as compared to tetroon (constant density balloon) trajectories and gaseous tracers under a wide variety of weather conditions, generally showed poor accuracy in sub-synoptic scale conditions (Hoecker, 1977; Pack et al., 1978; Warner et al., 1983; Clark et al., 1983; Haagenson, 1987).

A number of investigators have tried to determine whether increasing the spatial density and/or temporal frequency of wind observations would lead to an increase in trajectory accuracy. The results are mixed. Clark et al. (1983) found trajectory accuracy, measured against tetroon trajectories, increased with an increase in the temporal resolution of observations, especially under complex

meteorological conditions. Kuo et al. (1985), using a 72-hour model simulation of an evolving cyclone, degraded the model for testing at various spatial and temporal resolutions, and also found that increased temporal resolution of the data set resulted in increased trajectory accuracy. On the other hand, Scott and Achtemeier (1987) increased the vertical structure as well as the temporal and spatial resolution of the meteorological data, and found that an increase in trajectory accuracy was most dependent on the height of the trajectory surface that was selected. Kahl and Sampson (1988) found that increasing the spatial resolution of the wind field increased the accuracy of trajectories only in the first 400 meters of the atmosphere. Their results suggest that increasing both the spatial and temporal resolution of the wind field was necessary to increase the accuracy of trajectories above 400 meters.

Unfortunately, it is not possible to improve the resolution of the wind data set used in this study. Given the coarse horizontal and temporal resolution of both the wind observations and the gridded data sets (obtained from integrating observations with NWP first-guess fields), large differences can potentially exist between actual and calculated trajectories.

Another factor affecting trajectory accuracy, described in Chapter 1, is the choice of artificial surface (isentropic, isobaric, etc.) on which airflow trajectories are calculated. Generally speaking, calculated airflow trajectories, regardless of the type of model from which they were produced, are most accurate in strong, steady zonal flow conditions, and least accurate when airflow is weak or

atmospheric conditions are unstable.

For this study, it is assumed that, although differences likely exist between actual and calculated trajectories, there is no systematic bias to the trajectory errors, and that the random trajectory errors will "average out" due to the large number of trajectories for the ten-year study period. Thus, it should be possible to identify from the trajectory climatology the major pathways and sources of airflow affecting northwest Ohio. However, as with all climatological studies, the results of this analysis must be interpreted cautiously in light of the limitations of the original data set and the computational procedures.

CHAPTER III

GIS METHODS

1. Overview

Residence time analysis, developed and utilized by Ashbaugh et al. (1984), is the primary approach employed in this study to analyze the spatial distribution of the airflow trajectories. Residence time analysis has previously been used by a number of investigators for determining the likely source regions of airflow (e.g., Henmi and Bresch (1985), Poirot and Wishinski (1986), Malm et al. (1990), Comrie (1994), Merrill (1994)). As described in Chapter I, the procedures of residence time analysis include 1) overlaying a grid on the trajectory domain, 2) counting the number of times that trajectory nodes "reside" in each grid square, and 3) mapping the frequency distribution by grid cell of the trajectory nodes. Ridges and peaks on the resulting frequency plots can then be interpreted as airflow pathways and source regions for the terminus point of the trajectories.

For this study, the residence time analysis approach was adapted for use with geographic information system (GIS) technology. GIS technology offers a powerful computer tool for integrating and analyzing large quantities of spatial data, such as airflow trajectories. However, no previous studies that I am aware of have applied GIS methods to residence time analysis, even though the different steps in residence time analysis, such as overlaying a grid and

summing the frequency of nodes in each grid cell, are ideally suited to GIS application.

2. Choice of GIS

The GIS chosen for this project is the IDRISI system (Eastman, 1992), a raster (i.e., grid-based) GIS which operates on a personal computer. The IDRISI system has a wide variety of analysis functions including transforming a grid from one map projection to another, overlaying vector data (such as a base map) on a grid, performing scalar operations on a grid, overlaying two grids, and calculating relevant statistics (such as central tendency and dispersion measures) for a grid.

IDRISI was employed in order to implement the residence time method as it was originally developed by Ashbaugh et al. (1984). In their study, Ashbaugh et al. considered a trajectory to be made up of nodes or points and then counted the number of nodes falling within grid cells. In actuality, however, a trajectory also can be considered a line segment or vector. In this case, the frequencies per grid cell would indicate the number of times a line segment crossed that cell. The advantage of Ashbaugh et al.'s "node" approach is its simplicity. The disadvantage is that trajectories may actually span across one or more grid cells but these grid cells may not be included in the frequency count since only the nodes are counted. The span between nodes of a trajectory can be large when: 1) the winds are strong, 2) the time-period between each grid node calculation is large, and 3) when a fine-scale grid overlay is employed. We expect, given

the fairly coarse grid employed (see next section), the relatively small (i.e., 6-hour) time period between nodes, and the large number of trajectories for the ten-year study period, that there will be little or no bias as a result of using a raster-based GIS. However, a future study of the comparative advantages and disadvantages of employing a raster-based or vector-based GIS system in airflow studies is certainly warranted.

3. Creation of raster images

a. Initialization of the raster images

The first step in the GIS analysis was to create, using the IDRISI module called INITIAL, a new "image" for each month of the year. A latitude-longitude grid reference system was selected for the raster images, since the trajectory nodes are expressed in terms of latitude and longitude coordinates. The boundaries of each image were defined as 142°W to 67°W and 10°N to 85°N. These boundaries were determined by the spatial distribution of all the trajectory nodes for the ten-year study period. The dimensions of the raster images in terms of the number of rows and columns was 150 x 150, yielding a grid resolution of approximately 0.5° latitude by 0.5° longitude. This resolution was chosen to correspond to the resolution of Ashbaugh et al.'s (1984) original study. An initial value of zero was then placed in each grid cell of the images.

b. Transfer of the trajectory node data

Next, the trajectory node data were added to the raster images for each month. A computer program was written (in the Fortran language) to read the trajectory database files and create monthly point vector files in IDRISI format for each corresponding monthly raster image file. Each point in these files is a 6-hour trajectory node in latitude and longitude coordinates. These point vector files were then transformed to GIS raster images using the IDRISI module POINTRAS. The output from this module included the frequency of trajectory nodes (i.e., points) falling within each of the grid cells of the raster images. Thus, at the end of this step in the data analysis, each grid cell contained a frequency count.

c. Transformation to an equal area projection

Once the monthly raster images containing the frequency counts of trajectory node data were created, the next step was to transform them to a grid referencing system that would come close to yielding grid cells of uniform area throughout the image. It was important to transform the images to this type of projection for an upcoming step. The transformation was accomplished by using the IDRISI module PROJECT. PROJECT performs projection transformations on raster and vector files from one geo-referencing system to another. In this case, PROJECT transformed raster images in latitude and longitude coordinates to raster images in Transverse Mercator projection coordinates using a nearest

neighbor resampling procedure. The IDRISI module AREA was then used to calculate the area of the grid cells in the raster images. It was determined that each grid cell had an area of 2233.33 square kilometers or 47.26 x 47.26 kilometers.

PROJECT was also used to transform a vector base map file from latitude and longitude coordinates to Transverse Mercator projection coordinates. The vector base map was initially exported from a mapping software package. The exported boundaries were then converted to a line vector IDRISI file format. This step required only minor editing of the boundary file.

4. Correction for central tendency

Interpretation of the frequency images is complicated by the pronounced clustering of points near the terminus location. This central tendency is due to the fact that each trajectory is constrained to pass through one of the grid cells immediately surrounding the terminus in order to reach the terminus. In other words, the closer a grid cell is to the terminus the more probable it will be that a trajectory will pass through it. As a consequence, "raw" grid cell frequencies are not directly comparable between cells located different distances from the terminus, and some "adjustment" to the cell frequencies is necessary in order to be able to identify source regions of airflow for the terminus.

As discussed in Chapter I, Poirot and Wishinski (1986) developed a method for correcting for the central tendency of trajectory nodes about the

terminus. Their method employs distance-based scaling factors applied to each grid cell in the image. The approach essentially is attempting to estimate the decrease in the probability that a trajectory will pass over a grid cell as the distance of the grid cell from the terminus increases. The factors, which are unitless, represent the ratios of the area of a ring (which has a width of a grid cell (ij), at a distance D(ij) from the terminus), to the area of a single grid cell. The ratio can be thought of as the number of equally probable grid cells (due to geometry) at a given distance from the terminus. The factor at the terminus grid cell is equal to 1, and factors increase with increasing distance from the terminus. Equation (1) was used to compute the scaling factors:

$$(1) \qquad F(ij) = \frac{p\,[(D(ij) + R/2)^2 - (D(ij) - R/2)^2]}{R^2}$$

where F(ij) is the scaling factor for grid cell (ij), D(ij) is the distance from the terminus to grid cell (ij), and R is the length of a grid cell side assuming square and uniform grid cells throughout the study area (Poirot and Wishinsky, 1986), and p is pi (3.1415...).

To implement Equation (1), a new image was first initialized (using IDRISI module INITIAL) with a constant value of zero in each cell. The POINTRAS module was then used to set the terminus grid square to a value of one using a vector file containing the terminus coordinates as a single point in the file. The IDRISI module known as DISTANCE was used next to calculate the distances of

each grid cell from the terminus grid cell (D(ij) in Equation (1)). The DISTANCE module measures the Euclidean distance between each grid cell and non-zero grid cells (indicating target features). In this case, since the terminus grid cell was set to a value of one, DISTANCE recognized this as the target feature, and an image was created where each grid cell contained the Euclidean distance (in grid reference units) to the terminus grid cell. The length of the grid cell side (R in Equation (1)) was taken as the square root of the area of a grid cell. In this case, R was equal to 47.26 kilometers, based on a grid cell area of 2233.33 square kilometers. Equation (1) was then implemented using the following steps:

1. Create a new image (X1) using the module SCALAR to add R/2 to each grid cell in D, the distance image. SCALAR performs scalar arithmetic on raster images by adding, subtracting, multiplying, dividing or exponentiating the grid cell values by a constant value.

2. Create a second image (X2), again using SCALAR, to subtract R/2 from each grid cell in the distance image (D).

3. Create images XX1 and XX2 using SCALAR to exponentiate, to the power of 2, the values in each grid cell in images X1 and X2.

4. Create another new image (Y1) by subtracting XX2 from XX1 using the module OVERLAY. OVERLAY is an IDRISI module which produces a new image from operations such as addition, subtraction, and multiplication, using data from two input images.

5. Create another image (Y2) using SCALAR to multiply each grid cell in Y1 by pi (3.1415...).

6. Create a final image (F), the scaling factors, using SCALAR to divide each grid cell in Y2 with the area of a single grid cell (R^2).

7. Multiply (using OVERLAY) each of the monthly frequency images by image F in order to create the adjusted monthly frequency images.

When interpreting the adjusted frequency maps presented in the next chapter, the reader should keep in mind that the adjustments were made based on the frequency values at the terminus point. In other words, the frequency values for the grid cells beyond the terminus point are inflated based on the distance each grid cell is located from the terminus point. The adjusted frequency values for grid cells distant from the terminus point are much larger than the unadjusted values. Again, this is due to basing the correction factor on the terminus point, where the unadjusted frequencies are large. Readers should not attempt to directly compare the absolute values of the adjusted and unadjusted frequency maps. Rather, attention should be focused on the similarity and differences in the spatial patterns.

5. Calculating weighted mean centers

Mean centers provide an additional tool for summarizing the spatial distribution of the 5-day back trajectory nodes. The mean center is the spatial

equivalent of the arithmetic mean and can be "extremely useful in portraying the movement of the center of a spatial distribution over time" (Clark and Hosking, 1986). The unweighted mean center is simply the average location of the points, whereas the weighted mean center approximates the center of gravity of the point data using the frequency of the point data (in this case trajectory nodes) as the weight. Thus, the weighted mean is pulled closer towards locations with higher frequencies giving a more precise mean center. For this study, weighted mean centers were calculated every 24 hours along the trajectories for both adjusted and unadjusted frequencies. The 24-hour interval, rather than a 6- or 12-hour interval, was chosen because it was found that a smaller interval did not visually add any more information or significantly change the position of the line connecting the weighted mean centers over the 5-day period.

First, monthly frequency images of the trajectory nodes at -24, -48, -60, -72, -84, -96, -108, and -120 hours along the trajectories were created, using the same procedures described above to create the original raster images. Next, the IDRISI module CENTER was used to calculate the weighted mean centers for each time period.

Once the mean positions were calculated for each time period, the centers (identified by latitude-longitude coordinates) were then edited into IDRISI line vector files with a separate file for each month. The mean centers for each 24-hour time period were then connected by line segments and overlaid onto the appropriate monthly frequency images.

6. Summary

Ashbaugh et al.'s (1984) residence time analysis for analyzing airflow trajectories, including modifications later made by Poirot and Wishinski (1986), proved to be readily adaptable to geographic information system technology. In addition, other analytical measures, such as weighted mean centers, that are easily calculated within GIS software, can be used to supplement the residence time analysis in order to better understand airflow. The results of the airflow analysis are presented in the following chapter.

CHAPTER IV

RESULTS AND DISCUSSION

1. Overview

As stated in Chapter I, the main objective of this thesis is to use trajectory analysis to prepare an air mass climatology for northwest Ohio and to compare the resulting climatology to those prepared using alternative methodologies. Conceptually, trajectory analysis is a more appropriate technique for preparing an air mass climatology, since air masses can actually be traced back to their general region of origin. The source region of an air mass and the path that an air mass travels may be more accurate indicators of air mass type than other qualities such as air temperature and moisture characteristics.

Consistent with this main view, this chapter focuses on the results of the monthly trajectory analyses. It contains two sections. In the first section, the results of the monthly trajectory analyses will be described using the unadjusted and adjusted frequency plot maps that resulted from the GIS analyses detailed in Chapter III. The terms "airflow corridor" and "corridor" are used throughout this chapter to describe the elongated concentrations of trajectory nodes seen on the frequency plots indicating preferred airflow pathways. The maps will be supplemented by the tables of monthly percentages of trajectory nodes in the four compass quadrants surrounding the terminus. The second section is concerned with developing a seasonal air mass climatology for northwest Ohio

based on the monthly findings from the previous section. This seasonal air mass climatology for northwest Ohio is then compared to previous air mass climatologies for the study site location that were prepared using alternative methodologies.

2. Description of Results

a. January

Both the unadjusted (Figure 9) and adjusted (Figure 10) frequency plots of the 6-hour trajectory nodes reveal a strong westerly component to the airflow trajectories terminating in northwest Ohio during January. A primary airflow corridor stretches west-to-east from the eastern Pacific and northern and central California to northwest Ohio on both plots. The considerable length of this corridor is a reflection of the strong circumpolar vortex during January (Harman, 1991). However, the sources of the air masses that actually reach northwestern Ohio should be interpreted cautiously, as the 850 mb pressure surface intercepts the ground in regions of high terrain. Low-level air masses that originate west of the Rocky Mountains may not reach northwest Ohio due to the mountain barriers. A more cautious interpretation is the western Plains and eastern slopes of the Rocky Mountains are an important source region for air masses affecting northwest Ohio in January.

Several secondary corridors are also evident on the frequency plots. One such corridor originates in northwest Mexico and Baja California, extends

through west Texas, and intersects the primary westerly corridor in the Central Plains. This secondary corridor is better portrayed on the adjusted rather than unadjusted frequency plot. Another secondary corridor originates north-northwest of the terminus point, just south of Hudson Bay in the Canadian provinces of Ontario and Manitoba. The north-northwesterly corridor is considerably better defined on the adjusted frequency map. On the unadjusted plot, the corridor is obscured somewhat by the high frequencies immediately surrounding the terminus point. The north-northwesterly corridor appears to have a considerably shorter length than either the westerly or southwesterly corridors present during January.

On both maps, there is an indication of a minor airflow corridor originating northeast of the terminus point in the Canadian province of Quebec. Another minor corridor, extending east of the terminus point toward the mid-Atlantic region, is evident on the unadjusted plot but not on the adjusted frequency map. Both plots indicate that airflow trajectories originating from the southeast and south of the terminus point are relatively infrequent during January.

The 24-hour weighted mean centers are almost identical for the two frequency plots and illustrate the dominance of the westerly airflow corridor. This "average" 5-day back trajectory originates in southeastern Idaho and stretches through Wyoming, South Dakota, and the southern parts of Minnesota, Wisconsin and Michigan.

Figure 9. Frequency of 6-hourly trajectory nodes in January. Solid line is trajectory of mean node centers.

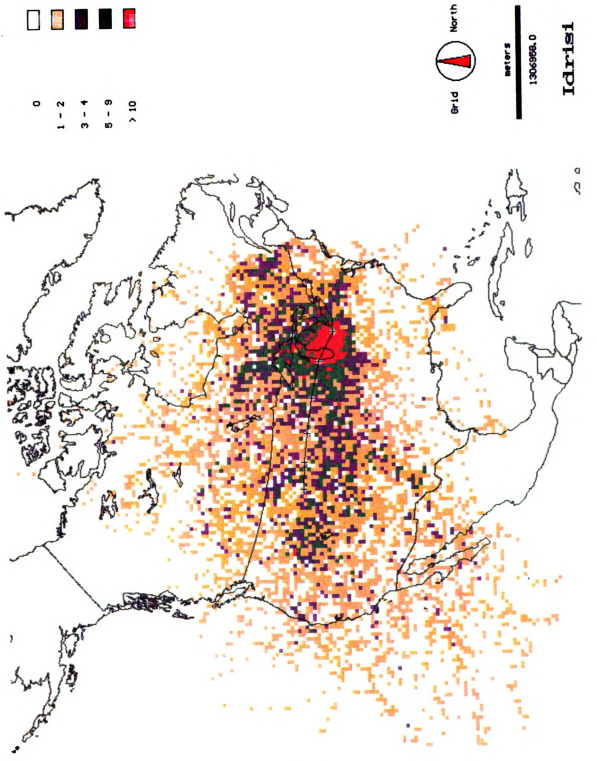

Figure 10. Frequency of 6-hourly trajectory nodes in January, adjusted for central tendency. Solid line is trajectory of mean node centers.

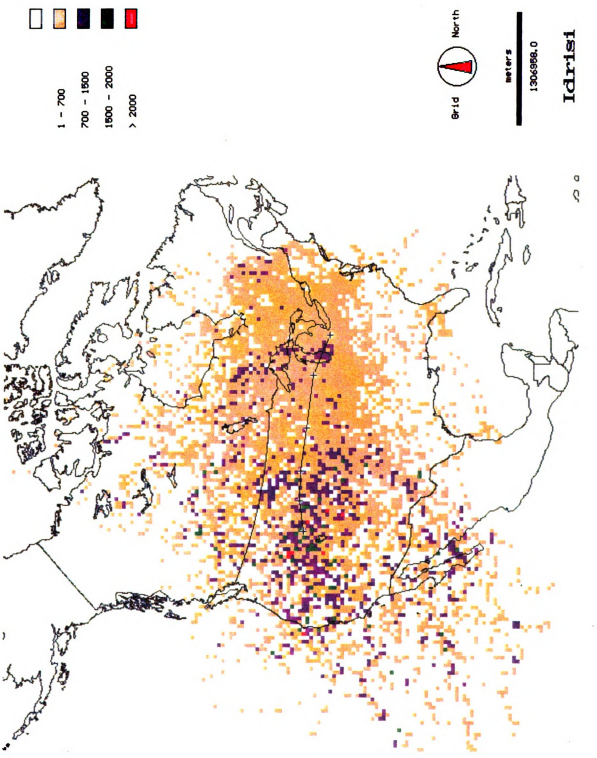

The percentage of trajectories by compass quadrant illustrates the difficulty of using this method to summarize airflow trajectories, as the importance of the westerly airflow corridor is masked in this summary. The data in Table 4 indicate that the majority of trajectory nodes were located in the northwest quadrant (53%), however, Table 5 indicates that 49% of the 5-day trajectories originated from the northwest quadrant. The second most important quadrant in January is the southwest, which contained 28% of all trajectory nodes (Table 4) and 35% of the -120 hour nodes. The northeast quadrant is also relatively important with 15% of the trajectory nodes and is the quadrant of origin for 13% of the trajectories. Only 4% of all trajectories nodes were located within the southeast quadrant.

b. February

The westerly and southwesterly airflow corridors present in January are not as clearly defined on the frequency plots for February. Instead, both the unadjusted (Figure 11) and adjusted (Figure 12) plots suggest that the 5-day trajectories terminating in northwest Ohio originate over a dispersed area across the western U.S. and the eastern Pacific. Readers are reminded that the suggested source regions west of the Rocky Mountain barrier should be interpreted cautiously.

Table 4

Percent of trajectory nodes by compass quadrant for twice daily airflow trajectories terminating at the study site (January, 1976 - December, 1985)

	Quadrant			
	NE	SE	SW	NW
Month				
January	15	4	28	53
February	7	1	23	69
March	4	0*	28	68
April	5	1	18	76
May	8	2	14	76
June	7	2	22	69
July	3	6	16	75
August	8	6	24	62
September	9	11	23	57
October	17	4	21	58
November	13	1	18	68
December	13	2	25	60

* the percentage was less than 0.5%

Table 5

Percent of -120 hour trajectory nodes by compass quadrant for twice daily airflow trajectories terminating at the study site (January, 1976 - December, 1985)

	Quadrant			
	NE	SE	SW	NW
Month				
January	13	3	35	49
February	4	0*	26	70
March	2	0	38	60
April	2	1	28	69
May	4	2	24	70
June	4	3	30	63
July	2	7	20	71
August	8	6	27	59
September	8	12	23	57
October	17	4	28	51
November	13	1	24	62
December	14	1	31	54

* the percentage was less than 0.5%

The most distinct airflow corridor in February originates north-northwest of the terminus point. This corridor, stretching into the Northwest Territories of Canada, has a considerably larger spatial extent than the similarly-oriented corridor present in January. As for January, this north-northwesterly corridor is much better depicted on the adjusted frequency plot compared to the unadjusted plot. There also is a suggestion on the frequency plots of a second corridor with a northwesterly orientation. This corridor is located farther west and extends from the Canadian prairie provinces into the upper Midwest of the U.S. The

preference for northwest flow at this time of year is influenced by the mean long wave pattern of ridging over western North America (Harman, 1991).

The minor airflow corridors from the northeast and east that were present in January are largely absent in February. Also, like January, airflow trajectories terminating in northwest Ohio in February rarely originate in the southeastern and southern U.S.

The average trajectory for February, based on the 24-hour weighted mean locations, has a slightly more northwesterly orientation compared to the average trajectory for January, originating near the Canadian border in western Montana. This trajectory illustrates the difficulty of using average trajectories to depict airflow, as the 24-hour weighted mean centers do not fall along any of the airflow corridors identified from the frequency plots. Rather, the average trajectory represents the midpoint of the broad area from the southwest to the northwest of the terminus point from which trajectories originate in February.

When the trajectory nodes are grouped by compass quadrant (Table 4), a much larger percentage (69%) of trajectory nodes are located northwest of the terminus point compared to January. This change reflects the better-defined northwesterly corridors in February. The other noticeable change is the decrease during February in the number of trajectory nodes in the southeast and, particularly, the northeast quadrants.

Figure 11. Frequency of 6-hourly trajectory nodes in February. Solid line is trajectory of mean node centers.

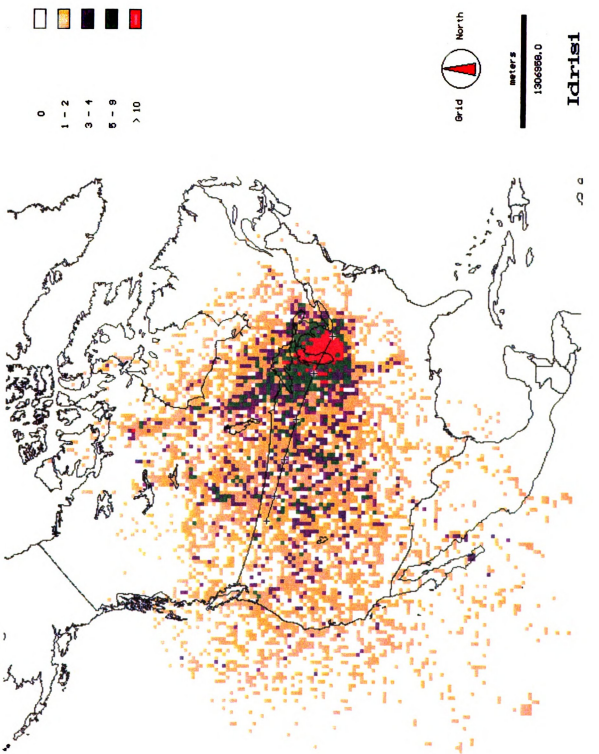

Figure 12. Frequency of 6-hourly trajectory nodes in February, adjusted for central tendency. Solid line is trajectory of mean node centers.

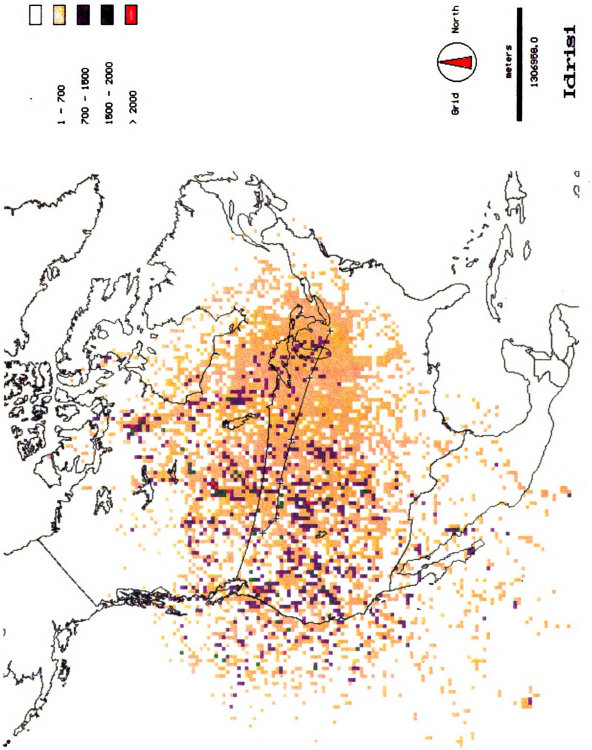

c. March

The north-northwest oriented airflow corridor evident during the previous months is even better defined and more spatially concentrated in March. This relatively narrow corridor, clearly evident on both the adjusted (Figure 13) and unadjusted (Figure 14) frequency plots, has a considerably greater extent in March, stretching from the northern reaches of the Northwest Territories of Canada into the upper Great Lakes region and then to the terminus point in northwest Ohio. In addition, both the adjusted and unadjusted plots suggest the presence of a secondary northwesterly corridor located to the west of the primary corridor. This secondary corridor, extending from approximately Great Slave Lake in Canada through the upper Midwest to the terminus point, is located somewhat farther east compared to a similar corridor evident in February. This shift in location of the northwesterly corridor and the strengthening of the north-northwest corridor agree well with the typical changes in the general circulation from February to March. In February the largest increases in the height of the 500 mb pressure surface (an indication of upper-level ridging in the large-scale circulation) occur over central Canada, whereas in March the largest height increases are centered over Hudson Bay. Consequently, there is also a shift eastward of the polar anticyclone track in March (Harman, 1987).

As in February, a dispersed "fan" of trajectory nodes is evident west of the terminus point, although this "fan" has shifted slightly more southwestward in

March, particularly on the adjusted frequency plot. This shift is supported by a modest increase in the percentage of trajectory nodes (from 23% in February to 28% in March) found in the southwest quadrant (Table 4), and a fairly substantial increase (from 26% in February to 38% in March) in trajectories which originated in the southwest quadrant five days prior to reaching the terminus (Table 5). In fact, this is the highest percentage for the year of trajectories originating in the southwest quadrant. Within this "fan" of trajectory nodes, there appears to be a modest indication of an airflow corridor originating in the southwest United States, similar to the southwesterly corridor observed in January. The exact source region of low-level airflow should be interpreted cautiously, however, as this area is a region of high terrain. The southerly airflow corridors suggests more frequent long wave troughing over western North America in March or split flow, although the modal pattern for this month is a ridge in the mean long wave pattern over western North America (Stark 1965; Harman, 1991).

A westerly corridor originating east of the Rocky Mountains also appears to be present. Trajectory nodes to the east and south of the terminus point are even more uncommon in March compared to the previous months. Only 4% of all trajectory nodes were in the northeast quadrant and less than half a percent of the trajectory nodes fell within the southeast quadrant (Table 4).

Figure 13. Frequency of 6-hourly trajectory nodes in March. Solid line is trajectory of mean node centers.

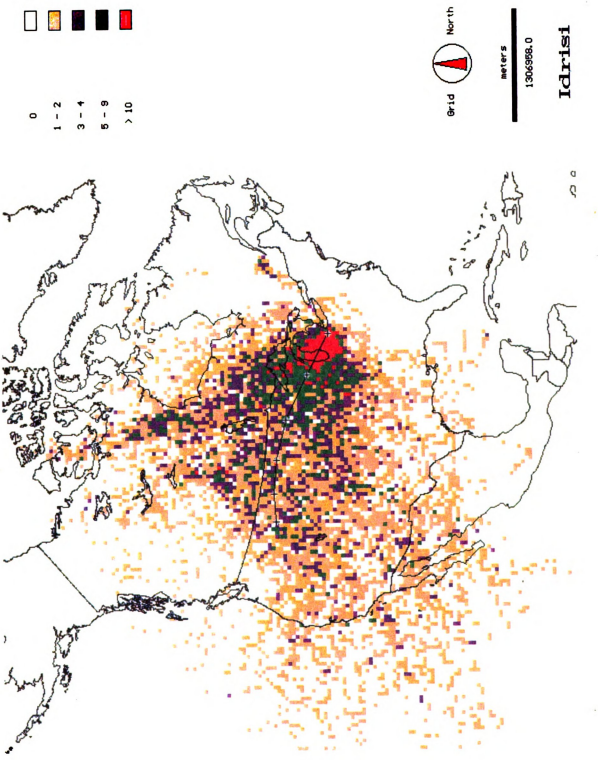

Figure 14. Frequency of 6-hourly trajectory nodes in March, adjusted for central tendency. Solid line is trajectory of mean node centers.

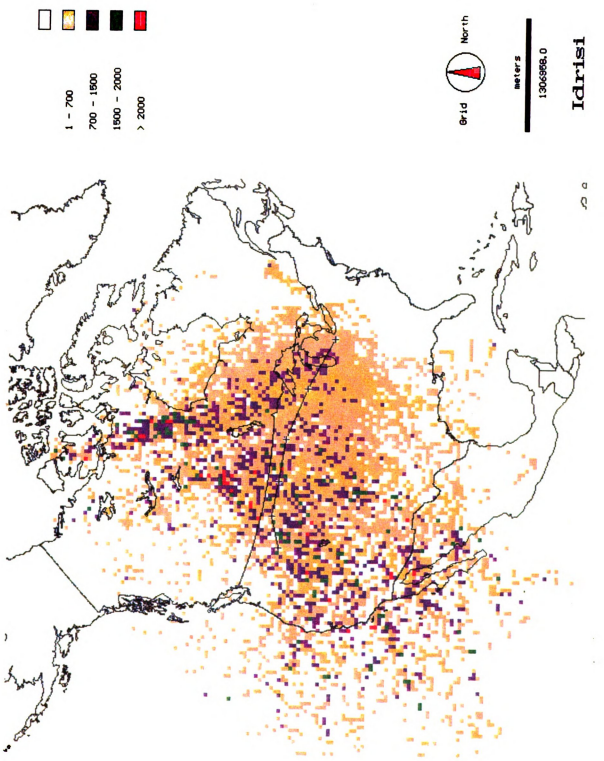

d. April

The distribution of the 6-hour trajectory nodes for April can be viewed as two large "fans," one extending from the terminus point toward the northwest and another extending toward the southwest of the terminus point. The northwestern fan is dominant on the unadjusted frequency plot (Figure 15) , although the two fans appear to be of approximately equal importance on the adjusted plot (Figure 16). As in March, split flow may be occurring over North America during this time of year (Harman 1991). The northern branch of the circulation is dominated by ridging over western and central Canada, whereas the southern branch is dominated by troughing over the western United States.

The previously-noted north-northwesterly and northwesterly airflow corridors can be discerned within the larger northwestern "fan" of nodes. Similar to the previous months, the north-northwesterly corridor is better defined compared to the northwesterly corridor. The location, extent, and spatial concentration of the north-northwesterly corridor during March and April are similar. In contrast, the northwesterly corridor is much more dispersed and extends from the Canadian prairies toward the terminus point. The importance of the north-northwesterly and northwesterly corridors during April is indicated by the large proportion (76%) of trajectory nodes that fell within the northwest quadrant (Table 4), as well as the large percentage of trajectories originating in this quadrant (69%) (Table 5).

Also apparent from Tables 4 and 5, the overall frequency of trajectory nodes falling in or originating within the southwest quadrant has decreased in April from the previous months, although the southwesterly airflow corridor has a similar appearance to the corridors evident in the previous months. As in March, few trajectory nodes were located in the northeast and southeast quadrants during April.

The difference between the average trajectories calculated from the adjusted and unadjusted frequencies is greater in April compared to the earlier months. For the unadjusted plot, the location and extent of the average trajectory primarily reflect the northwestern airflow corridors. On the other hand, the influence of both the northwestern and southwestern corridors is evident on the average trajectory calculated from the adjusted frequencies. For Days 1 and 2 of the back trajectory (i.e., the 24-hour weighted mean centers located in Wisconsin and Minnesota), the average trajectory is representing the northwesterly corridors. By Day 5, the location of the weighted mean center in southwestern Idaho is predominantly influenced by the longer southwesterly trajectories.

e. May

The weakening of the general circulation as the Northern Hemisphere warms is evident from the frequency plots for May (Figures 17 and 18). The

Figure 15. Frequency of 6-hourly trajectory nodes in April. Solid line is trajectory of mean node centers.

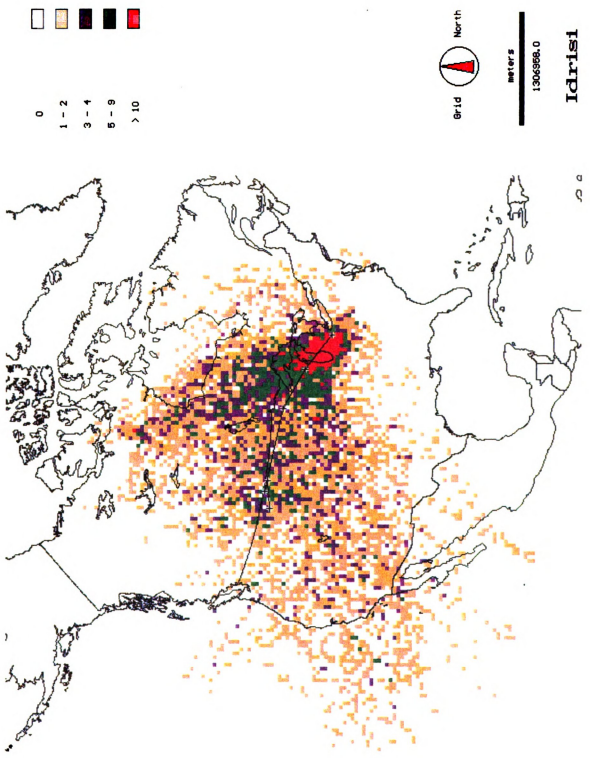

Figure 16. Frequency of 6-hourly trajectory nodes in April, adjusted for central tendency. Solid line is trajectory of mean node centers.

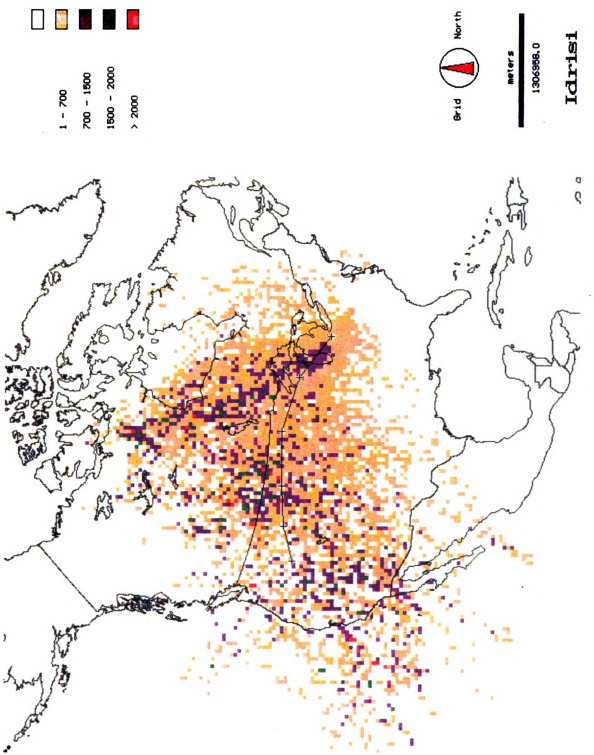

farthest northward, westward, and southward extent of the trajectory nodes in May is considerably less than that for the previous months.

Once again the most distinct feature of the plots for May is the north-northwesterly airflow corridor. This corridor is somewhat shorter compared to similar corridors in March and April, extending to the west and southwest of Hudson Bay. However, the frequency of nodes along the corridor in May is higher compared to the earlier months. The more dispersed northwesterly corridor originating in the Canadian prairie provinces is also present in May. The dominance of northwesterly trajectories is confirmed by Tables 4 and 5. Over 75% of the trajectory nodes fell within the northwest quadrant in May, and 70% of the trajectories originated there.

Two relatively weak corridors with southwesterly orientations are also evident in May. One corridor originates in west Texas, and the other originates in central California and/or southern Colorado. However, the southwest quadrant is a less important source region for airflow in May compared to previous months. In fact, the proportion of trajectory nodes in this quadrant reaches its lowest percentage for the year in May (14%) (Table 4). Only 24% of the trajectories originated from the southwest quadrant (Table 5). The smaller number of southwesterly trajectories is also evident in the placement of the average trajectory, which is located considerably farther north and northwest compared to the previous months.

Figure 17. Frequency of 6-hourly trajectory nodes in May. Solid line is trajectory of mean node centers.

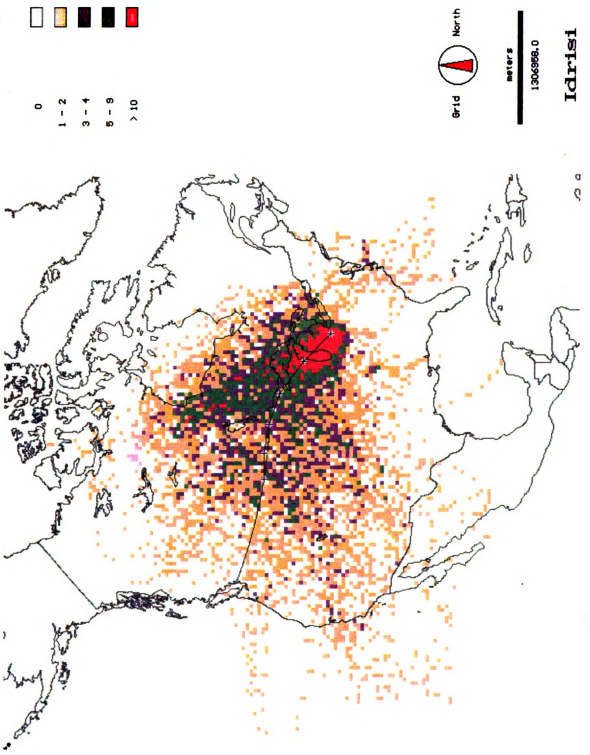

Figure 18. Frequency of 6-hourly trajectory nodes in May, adjusted for central tendency. Solid line is trajectory of mean node centers.

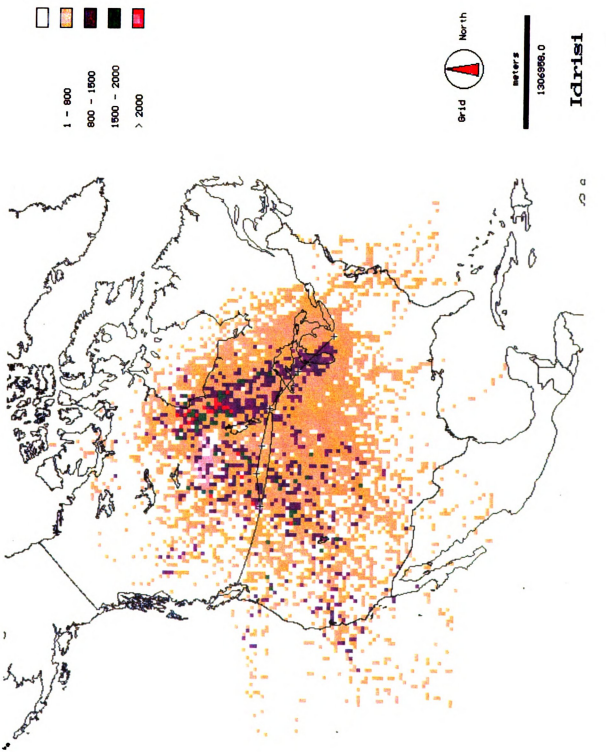

f. June

The major feature of the June plots (Figures 19 and 20) of the trajectory nodes is the increase in the frequency of southwesterly trajectories from May. Note, in particular, the concentrations of nodes in northwest Texas and northeastern New Mexico and in central and southern Colorado. The increased importance of the southwesterly trajectories is also indicated in Tables 4 and 5. The proportion of trajectory nodes in the southwest compass quadrant increases by 8 percent from May to June, and the percentage of trajectories originating in this quadrant increases from 24% in May to 30% in June. Furthermore, the southward shift in the 24-hour weighted mean centers (i.e., the location of the average trajectory) is an indication of more frequent southwesterly trajectories in June compared to May.

Although the north-northwesterly quadrant remains clearly evident in June, its length continues to decrease. The largest concentration of nodes is now located in southwestern Ontario. There is a secondary concentration of nodes in southern Saskatchewan that reflect the northwesterly corridor present during the previous months. However, this corridor is very spatially dispersed in June.

Figure 19. Frequency of 6-hourly trajectory nodes in June. Solid line is trajectory of mean node centers.

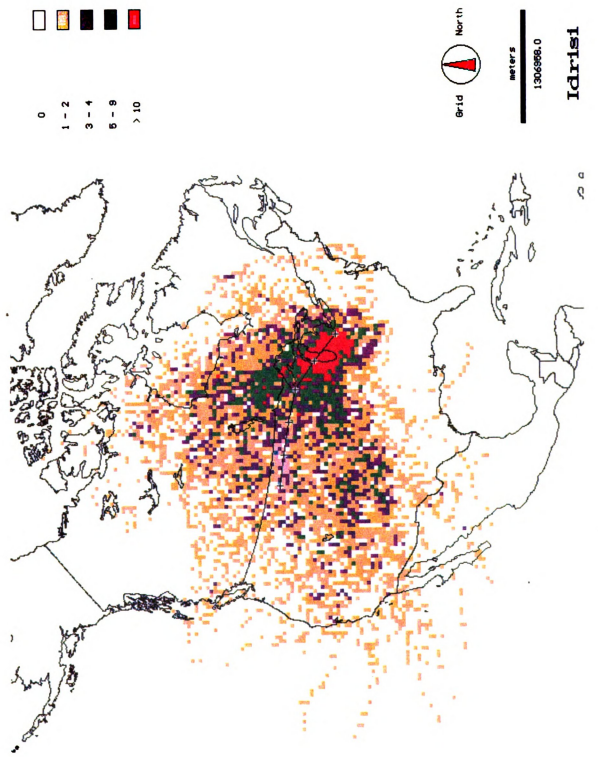

Figure 20. Frequency of 6-hourly trajectory nodes in June, adjusted for central tendency. Solid line is trajectory of mean node centers.

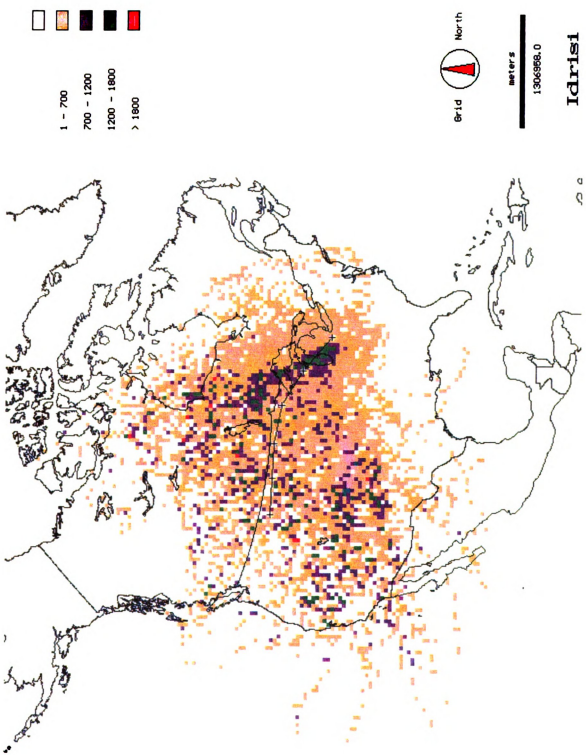

g. July

The compactness of the trajectory node locations in July is evidence of the continued weakening of the general circulation during the North Hemisphere summer (Figures 21 and 22). The north-northwesterly corridor is still the most pronounced although it continues to shrink in length. Secondary, spatially dispersed northwesterly and westerly corridors are also evident in the frequency plots. Table 5 confirms this observation. The percentage of trajectories originating in the northwest quadrant has reached a maximum for the year in July at 71%. On the other hand, the southwesterly corridor that was present in June is much weaker in July. In fact, the proportion of trajectories originating from the southwest quadrant is smallest (20%) in July compared to any other month (Table 5). The average trajectory aligns fairly well with the secondary westerly corridor, especially on the unadjusted frequency map.

The shift from southwesterly to more westerly and northwesterly airflow corridors is in concordance with the upper-level ridging that typically occurs over the western U.S. in summer due to continental heating that suppresses troughing in this region (Harman, 1991). The mean anticyclone track for July also changes from the preferred polar track of previous months to the more westerly Pacific track (Harman, 1987).

A striking feature of the July frequency plots is the infrequent occurrence of northeast trajectories. Table 4 indicates that the proportion of trajectory nodes which fell within the northeasterly compass quadrant is at a minimum in July

(3%). On the other hand, trajectory nodes in the southeast compass quadrant increased in July. A minor airflow corridor extends from the terminus point southeastward into southern Ohio and Kentucky on the adjusted frequency plot and as far as the southeastern Atlantic coast on the unadjusted frequency plot.

h. August

The frequency plots of the trajectory nodes (Figures 23 and 24) are considerably more complex in August compared to July. A larger number of airflow corridors are evident, which appear as multiple "spokes" emanating from the terminus point.

Perhaps the most interesting change from July to August is the strengthening of the airflow corridor located south and southeast of the terminus point. The southerly corridor is best defined in August compared to any of the other months of the year. Although the corridor does not have a large spatial extent, the number of nodes falling along the corridor is fairly large.

Another "spoke of the wheel" is the easterly corridor extending into southern New England, particularly on the unadjusted frequency plot. This corridor has largely been absent in all the previous months except January. Continuing counterclockwise, the north-northwesterly corridor, although still evident, is weaker than previous months and is also located slightly farther west. The westward shift of this corridor likely reflects the weak upper-level ridge typically present over central North America in August (Harman, 1991).

Figure 21. Frequency of 6-hourly trajectory nodes in July. Solid line is trajectory of mean node centers.

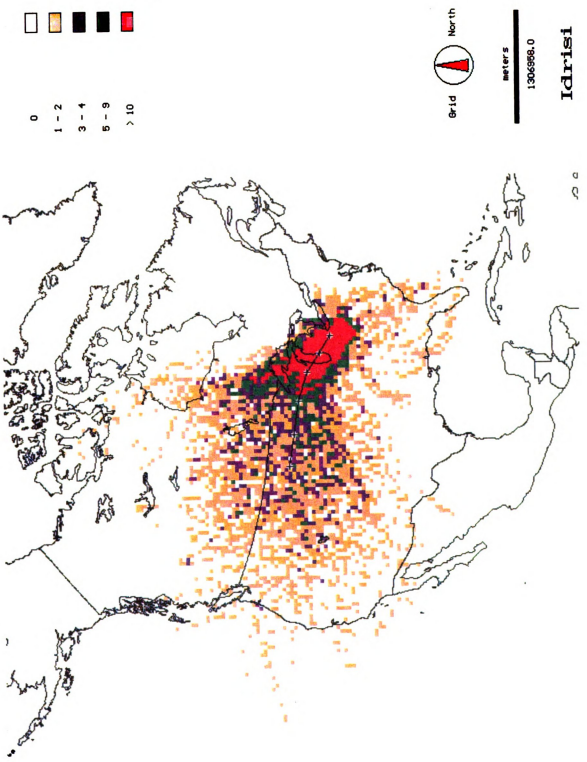

Figure 22. Frequency of 6-hourly trajectory nodes in July, adjusted for central tendency. Solid line is trajectory of mean node centers.

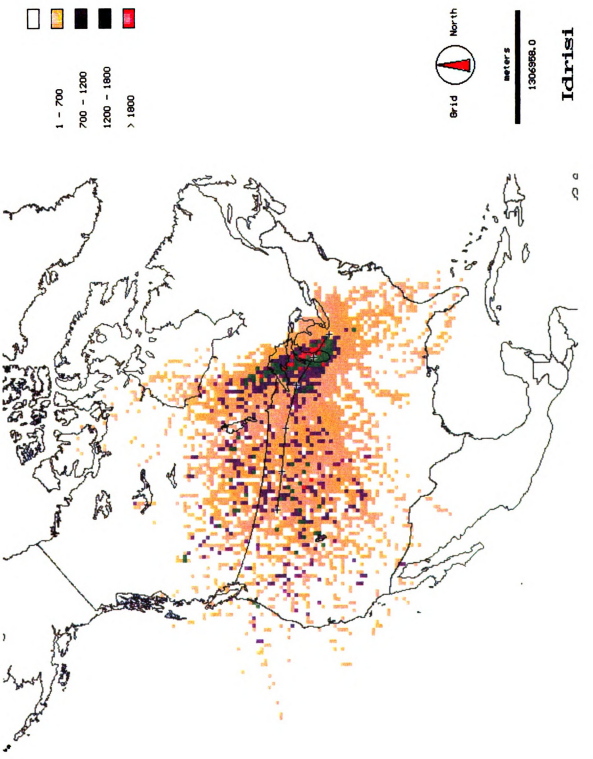

Figure 23. Frequency of 6-hourly trajectory nodes in August. Solid line is trajectory of mean node centers.

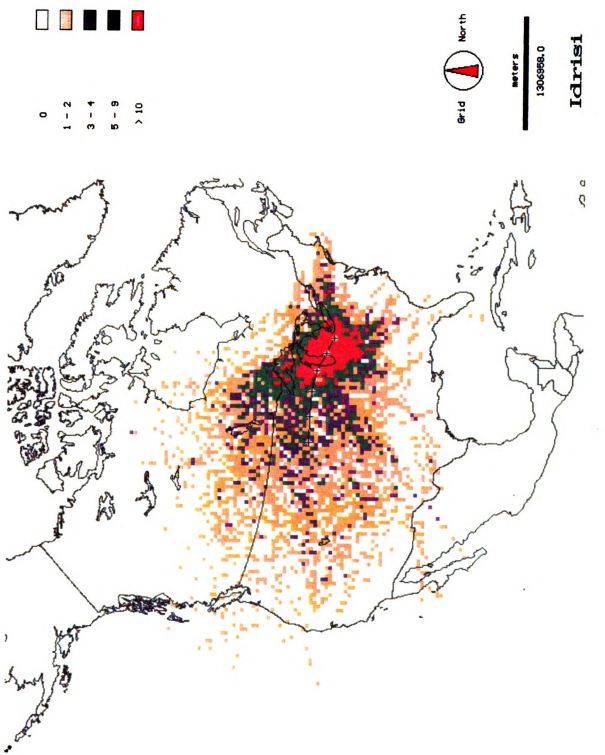

Figure 24. Frequency of 6-hourly trajectory nodes in August, adjusted for central tendency. Solid line is trajectory of mean node centers.

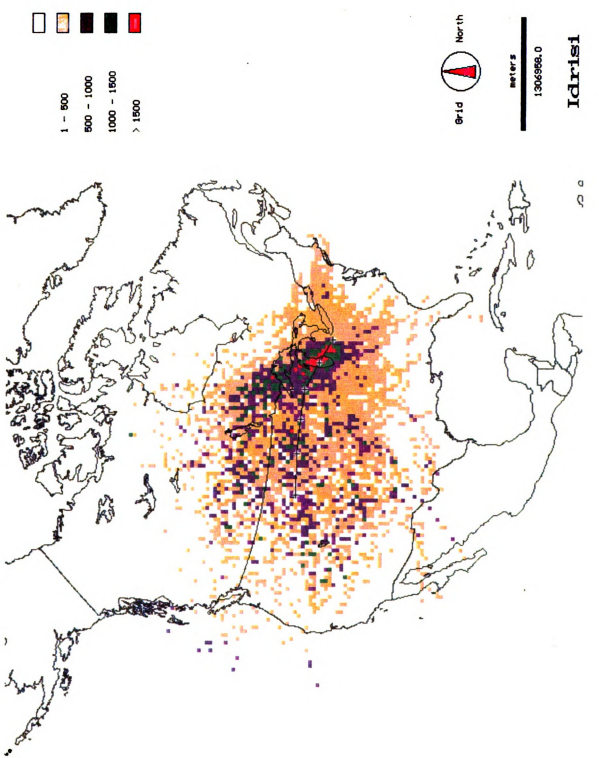

Fairly well-defined airflow corridors are also evident to the west and southwest of the terminus point. Both these corridors have longer extents compared to the southerly, easterly, and north-northwesterly corridors.

Not surprisingly, given the spatial pattern of the trajectory nodes, the frequency of trajectory nodes in the northeast and southwest quadrants increases from July to August, whereas the number of trajectory nodes in the northwest quadrant decreases (Tables 4 and 5). The average trajectory is located farther south in August compared to any other month except January. Similar to July, the average trajectory aligns fairly well with the westerly airflow trajectory.

i. September

The north-northwesterly corridor continues to weaken in September, whereas a northwesterly corridor originating considerably farther west over the Canadian prairie provinces strengthens during this month (Figures 25 and 26). On the other hand, the westerly and southwesterly corridors are not as distinct as similar corridors present in August. These changes are consistent with the ridging over western Canada and troughing over Hudson Bay, which is the typical upper-level flow pattern in September (Stark, 1965; Harman, 1991). A change is also evident in the easterly corridor. This corridor has shifted somewhat southward in September compared to August and now has a more east-southeasterly orientation. This shift in location is reflected in the monthly

percentages of trajectory nodes residing and/or originating in the southeast compass quadrant (Tables 4 and 5). Note that the percentages for the southeast quadrant reach their maximum in September. Finally, a surprisingly strong but small source region of airflow in September is present along the northern tip of the Yucatan Peninsula of Mexico, almost due south of northwest Ohio. Both the east-southeasterly and southern corridors are more difficult to explain in terms of the typical upper-level geopotential height patterns for September. These southerly air streams may be the "warm conveyor belt" of cyclones.

There is considerable discrepancy in the locations of the 24-hour mean centers calculated from the adjusted and unadjusted frequencies. The average trajectory calculated from the adjusted frequencies has a more northerly location and longer spatial extent. It aligns fairly well with the northwesterly airflow corridor originating in the Canadian prairie provinces. On the other hand, the average trajectory calculated from the unadjusted frequencies, extending from northern South Dakota through central Wisconsin to the terminus point, represents the approximate midpoint of the fan of trajectory nodes to the west and northwest of the terminus location.

Figure 25. Frequency of 6-hourly trajectory nodes in September. Solid line is trajectory of mean node centers.

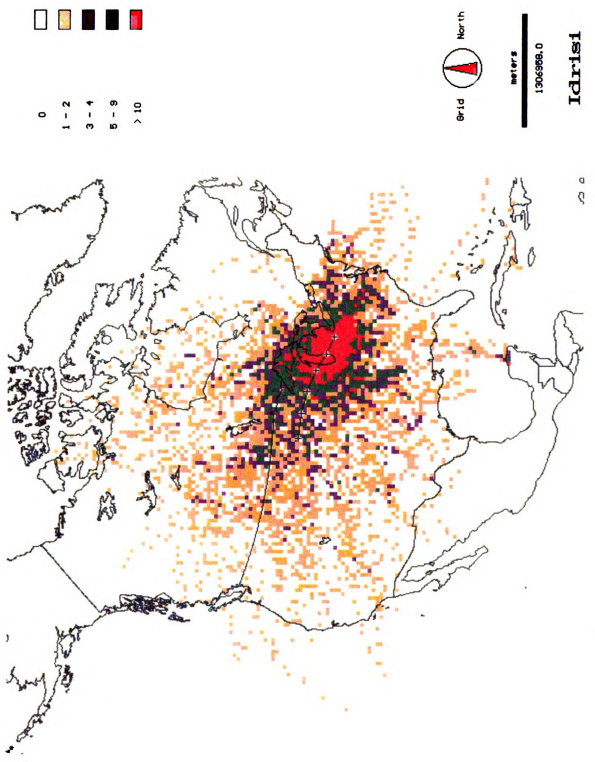

Figure 26. Frequency of 6-hourly trajectory nodes in September, adjusted for central tendency. Solid line is trajectory of mean node centers.

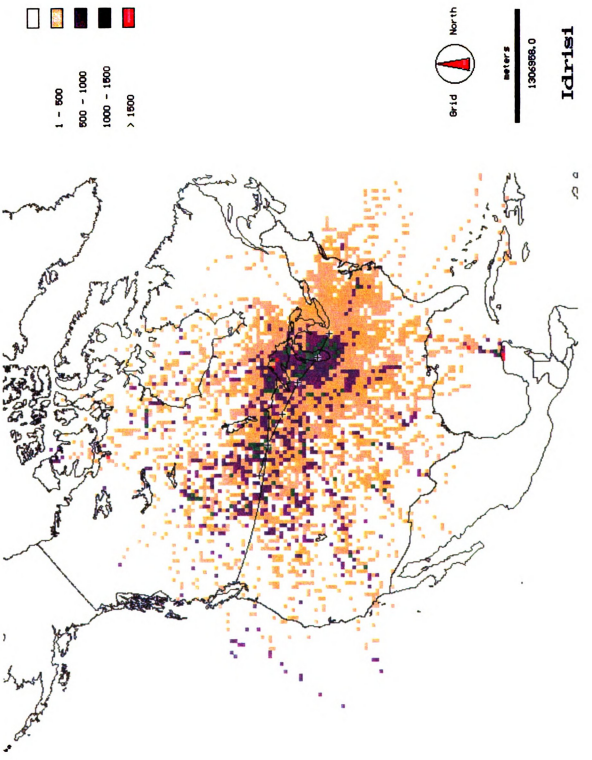

j. October

The frequency plots for October are characterized by a lack of distinct airflow corridors. On both the unadjusted (Figure 27) and adjusted (Figure 28) plots, the greatest frequency of trajectory nodes is found immediately west and northwest of the terminus point. This pattern suggests that most trajectories during October have fairly short lengths. However, less frequent, longer length trajectories from the west and southwest are also evident on the frequency plots. These longer trajectories may be occurring later in the month, when middle and upper-level wind speeds increase due to the increased temperature gradient across the North American continent.

An interesting feature in Table 4 is the relatively large percentage (17%) of trajectory nodes in the northeast compass quadrant. This value, which is larger for October compared to any other month, appears to reflect a weak airflow corridor extending from the terminus point into eastern Ontario and western Quebec. This corridor is better defined on the unadjusted frequency plot. The plotting of representative trajectories for this month suggests the northeast airflow pattern is caused by the anticyclonic curvature of westerly trajectories flowing to the north and east of the study site, then curving back in a clockwise manner before terminating in northwest Ohio, perhaps associated with flow into a cyclone. As expected given the relatively dispersed pattern of the frequency nodes, the average trajectories calculated from both the adjusted andunadjusted frequencies do not lie along distinct airflow corridors.

Figure 27. Frequency of 6-hourly trajectory nodes in October. Solid line is trajectory of mean node centers.

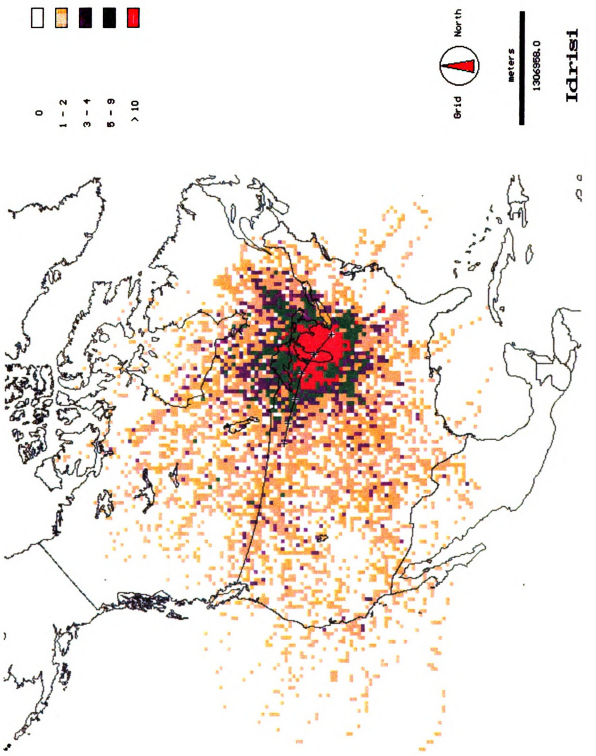

Figure 28. Frequency of 6-hourly trajectory nodes in October, adjusted for central tendency. Solid line is trajectory of mean node centers.

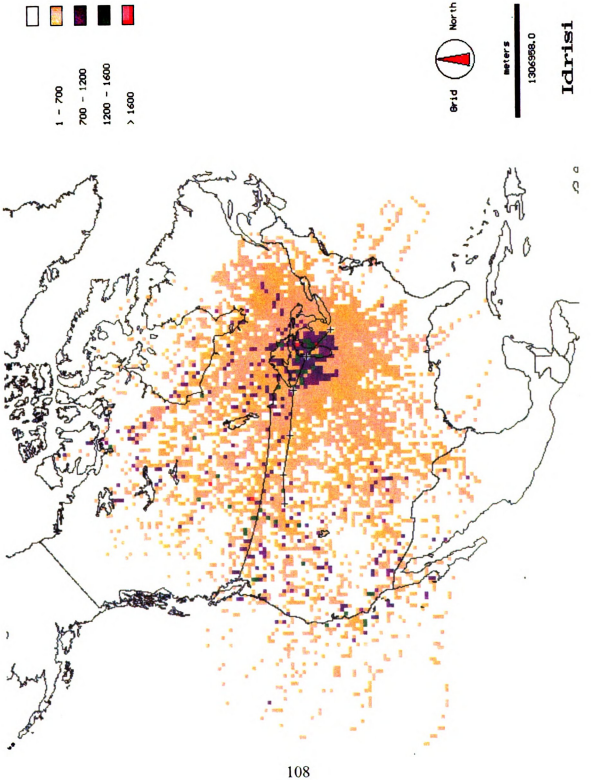

k. November

November is marked by the return of a distinct north-northwesterly airflow corridor. Not only is the frequency of trajectory nodes along this corridor large, but the corridor extends well north of the Arctic Circle (Figures 29 and 30). The extent of the corridor is similar to that observed earlier for the months of February-April. Also evident is a northwesterly airflow corridor extending from northern Alberta into central Saskatchewan. Both corridors are reflected in the 10% increase in the number of trajectory nodes which fell in the northwest compass quadrant (Table 4). The importance of these northwesterly corridors is also evident in the locations of the average trajectories. For both the unadjusted and adjusted frequencies, the average trajectories in November are located considerably farther north than in October and have a more northwesterly orientation. Both corridors are consistent with the average upper-level geopotential height pattern for November, which is characterized by ridging over western Canada and troughing over eastern Canada and the northeastern U.S. (Harman, 1991). In addition, the mean anticyclone track shifts from Pacific to polar in November (Harman, 1987).

The percentage of trajectory nodes in the northeast compass quadrant is relatively large in November compared to the other months, although less than the maximum observed in October (Table 4). The source region for these trajectories appears to be north and northeast of Lake Ontario in southwestern Quebec. However, as in October, this corridor is mainly the result

of anticyclonic curvature of westerly trajectories. On the other hand, southeast quadrant trajectory nodes are infrequent in November. Airflow corridors to the west and southwest are evident on the frequency plots, as was the case for many of the previous months. Similar to October, trajectories originating from these areas tend to have considerable lengths, as expected given the strengthening upper-level flow.

l. December

The north-northwesterly airflow corridor in December does not have as great a spatial extent as the corridor present in November (Figures 31 and 32). Also, the frequency of trajectory nodes along this corridor is not as large in December. At the same time, the northwesterly airflow corridor has increased somewhat in extent, although there appears to be little change in frequency. Another change since November is the increased frequency of trajectory nodes to the west and southwest, particularly over the central Rockies and central Plains and over the southwestern U.S. The quadrant percentages (Tables 4 and 5) confirm these shifts in trajectory node location. The number of trajectory nodes falling within or originating from the northwest compass quadrant decreases by approximately 8% from November to December, whereas the percentage of trajectory nodes in the southwest compass quadrant increases by approximately the same amount. The middle and upper-level average geopotential height patterns for November and December provide little

Figure 29. Frequency of 6-hourly trajectory nodes in November. Solid line is trajectory of mean node centers.

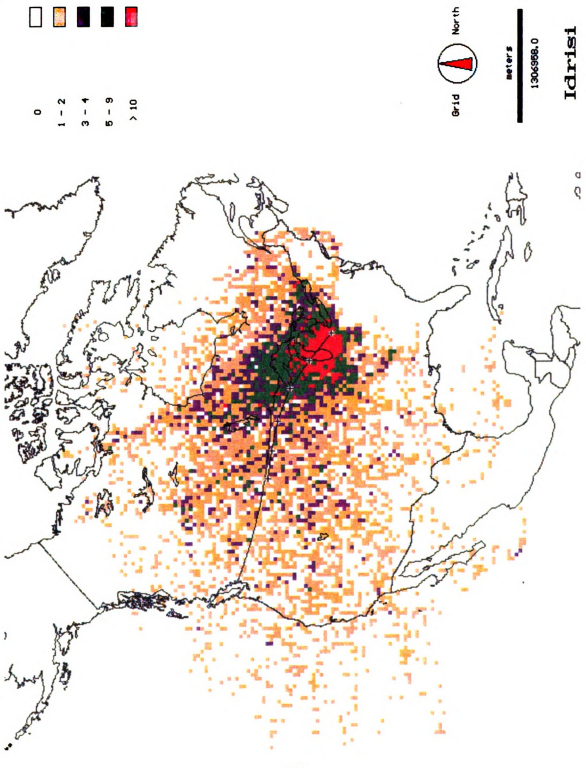

Figure 30. Frequency of 6-hourly trajectory nodes in November, adjusted for central tendency. Solid line is trajectory of mean node centers.

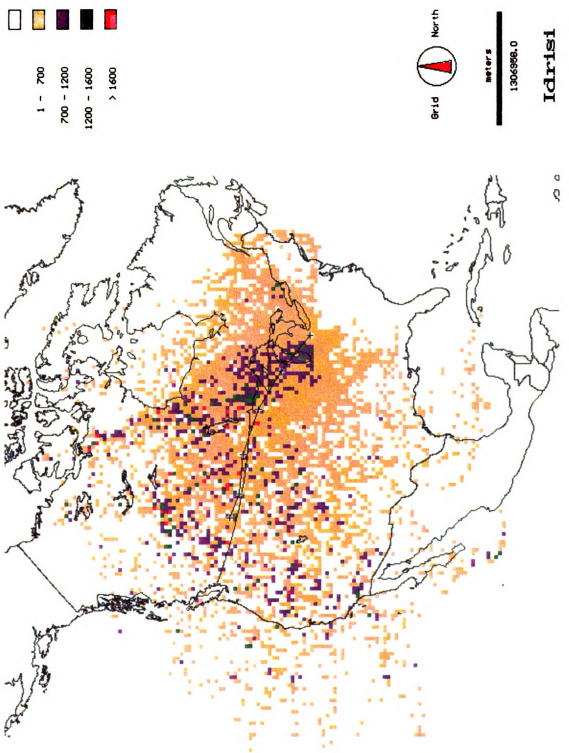

insight on the reasons for the shifts in the airflow corridors from November to December. For both months, the average geopotential height patterns are characterized by ridging over western North America and troughing over eastern North America (Harman, 1991).

The greater frequency of southwesterly trajectories is also evident from the location of the 24-hour weighted mean centers. For both the unadjusted and adjusted frequencies, the average trajectory is located farther south in December compared to November and has a more westerly orientation, originating at the eastern base of the Rocky Mountains in central Montana and stretching through the Dakotas, Minnesota, Wisconsin, and Michigan. As usual, the average trajectories do not align with any of the corridors evident from the frequency plots.

Trajectory nodes in the southeast compass quadrant remain infrequent in December. However, both the unadjusted and adjusted plots suggest that the northeasterly corridor, observed in October and November, is still present. This corridor appears to extend somewhat farther northeast into eastern Quebec compared to a similar corridor evident in November, but is caused by similar events as in October and November, i.e., the anticyclonic curvature of westerly trajectories.

Figure 31. Frequency of 6-hourly trajectory nodes in December. Solid line is trajectory of mean node centers.

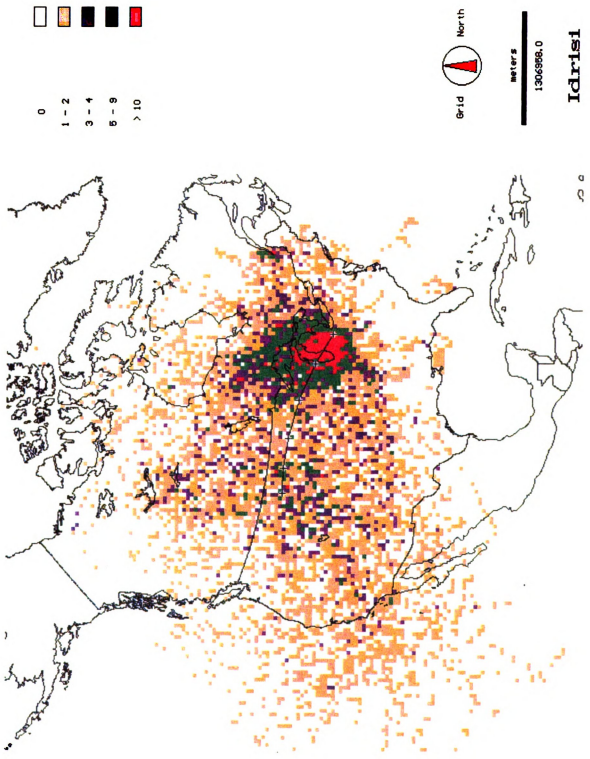

Figure 32. Frequency of 6-hourly trajectory nodes in December, adjusted for central tendency. Solid line is trajectory of mean node centers.

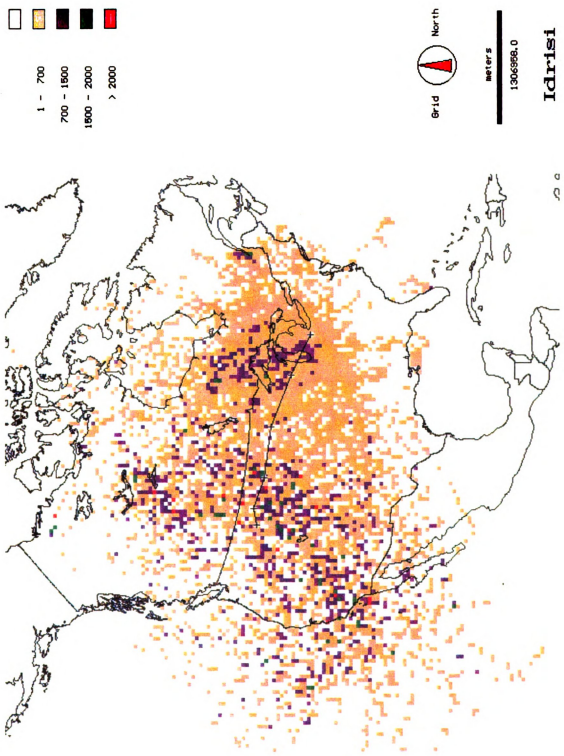

3. Aggregation by season and comparison to previous studies

The monthly trajectory analyses results from the previous section were aggregated by seasons and associated with air mass types in order to develop a seasonal air mass climatology that can be more easily compared with the findings of previous studies.

a. Air mass names

Air mass "names" were given to each of the prominent corridors identified in the frequency maps. The names reflect the source regions (e.g., furthest extent) of the 5-day back trajectories. The names have implied temperature and moisture properties and can be described as follows:

Arctic - Air masses originating in the Canadian Arctic archipelago and the Arctic Ocean. This air mass type is transported to northwest Ohio by the well-defined north-northwesterly airflow corridor. The air mass type is most comparable to Brunnschweiler's (1952) "Continental Arctic" air mass and Borchert's (1950), Bryson's (1966) and Wendland and Bryson's (1981) "Arctic" air mass.

Canadian - Air masses originating in central Canada. This air mass name is used here to identify air masses transported to northwest Ohio along the spatially-dispersed northwesterly corridor. The Canadian air mass type appears most like Brunnschweiler's (1952) "Continental Polar" air mass, and Schwartz's (1982; 1991) and Schwartz et al.'s (1985) "Polar"

air mass type for summer and their "Continental" air mass type for the remaining seasons.

Pacific - Air masses originating from the north Pacific Ocean that have traversed the Rocky Mountains, thereby becoming warmer and drier. This air mass type is transported to northwest Ohio in the dispersed westerly airflow corridor. It also includes any source regions along this axis, such as the lee of the Rocky Mountains. The Pacific air mass type is similar to Brunnschweiler's (1952) "Maritime Polar" air mass, and Schwartz's (1982;1991) and Schwartz et al.'s (1985) and Bryson's (1966) "Pacific" air mass type. It is also similar to Borchert's (1950) source region termed "the eastern base of the Rocky Mountains", and Wendland and Bryson's (1981) source regions termed "north Pacific Ocean" and "High Plains".

Southwest - Air masses originating in the southwest U.S. and Mexico, and further westward over the Pacific Ocean. These air masses are transported to northwest Ohio by the southwesterly airflow corridor. This air mass type is likely similar to Brunnschweiler's (1952) "Continental Tropical" and Schwartz's (1982;1991) and Schwartz et al.'s (1985) "Dry Tropical" air mass designations.

Tropical - Air masses originating in the Gulf of Mexico or Atlantic Ocean off the coast of the southeastern United States. This air mass type is transported to northwest Ohio by the southeasterly and southerly airflow

corridors. It is comparable to Brunnschweiler's (1952) "Maritime Tropical" air mass type, Schwartz's (1982;1991) and Schwartz et al.'s (1985) "Tropical" air mass type, and the source region termed "sub-tropical Atlantic anticyclone" by Borchert (1950).

Atlantic - Air masses originating in eastern U.S. and Canada and transported to northwest Ohio by the easterly and northeasterly airflow corridors. A few of the trajectories have ~120 hour nodes over the Atlantic Ocean. This air mass name may be comparable to Bryson's (1966) Atlantic air mass type. Many of the trajectories in this airflow corridor originated in the west and curved back to northwest Ohio in the area of eastern Ontario and western Quebec. These trajectories were not given an air mass name.

b. Winter (December-February)

As discussed in Chapter I, the results of the earlier airflow-based climatologies for the winter months of December-February differed considerably from the results of the temperature/moisture-based air mass climatologies. The airflow-based studies suggest that northwestern Ohio is influenced by a large number of different air mass types in winter. Both Borchert (1950) and Bryson (1966) found that a marked confluence zone lies over northwestern Ohio in winter. These results suggest that air masses from the Pacific, the interior of Canada, and the Gulf of Mexico are equally important. Wendland and Bryson

(1981) found that, additionally, air masses originating over the nearby southern Ohio Valley and the High Plains are important at this time of year, particularly in early winter. In contrast, the temperature/moisture-based studies of Brunnschweiler (1952), Schwartz (1982;1991), and Schwartz et al. (1985) all found that continental air masses originating from interior Canada were dominant over northwest Ohio during winter. In fact, Schwartz (1982) and Schwartz et al. (1985) indicated that approximately 70 percent of the air masses affecting northwest Ohio in January were from continental sources, and Brunnschweiler (1952) found that continental polar air masses occurred 80 percent of the time.

The results of the trajectory analyses presented here support the findings that in winter northwest Ohio experiences a variety of air mass types during winter, but that the air masses are predominantly continental in origin. Important source regions, based on the 5-day back trajectories, were identified to the southwest, west, northwest and north-northwest of the terminus center. These regions would be sources of Southwest, Pacific, Canadian, and Arctic air masses, using the nomenclature defined above. In contrast to the studies of Borchert (1950) and Bryson (1966), the results of this study suggest that tropical and Atlantic air masses are infrequent in winter. This study also identifies important within season variations that were not previously noted. For example, Canadian and Arctic air masses are more frequent in late winter compared to early winter, whereas Pacific and southwest air masses are more frequent in early winter. Atlantic air masses are also more likely in early winter, and tropical

air masses, although infrequent, are most likely in January.

c. Spring (March-May)

The results of this study suggest that, similar to winter, Arctic, Canadian, Pacific, and Southwest air masses are dominant during spring over northwest Ohio. Arctic air masses, in particular, appear to be frequent at this time of year. On the other hand, Atlantic and tropical air masses are infrequent, especially in April. These results are in conflict with those of the previous air mass climatologies, particularly in regard to the frequency of tropical air masses. Both Bryson's (1966) and Borchert's (1950) streamline analyses suggest that as spring progresses the confluence zone lying over northwest Ohio in winter shifts northward, resulting in the more frequent occurrence of maritime tropical air masses. Wendland and Bryson's (1981) results also suggest that tropical air masses are important, as their analyses indicate that northwest Ohio is located close to a confluence zone of air streams from the Arctic and from the Atlantic. Schwartz's (1982) and Schwartz et al.'s (1985) results indicate that in spring the frequency of continental air masses decreases dramatically with an accompanying increase in the frequency of Pacific and dilute tropical air masses.

d. Summer (June-August)

Many of the previous air mass climatologies found tropical air masses to be dominant in northwest Ohio during summer. Bryson's (1966), Wendland and

Bryson's (1981), and Borchert's (1950) streamline analyses all suggest that northwest Ohio is primarily influenced by maritime tropical air originating from the Gulf of Mexico or the Caribbean Sea. Schwartz (1982;1991) and Schwartz et al. (1985) indicate that tropical air masses and transitional conditions are equally important in summer, each occurring on average from 25-30% of all days. Brunnschweiler's (1952) results show northwest Ohio to be a "conflict region" between continental polar and maritime tropical air masses.

In contrast, the trajectory analyses presented here suggest that, similar to winter and spring, Arctic, Canadian, Pacific, and Southwest air masses are dominant over northwest Ohio in summer. Tropical and Atlantic air masses are more frequent in mid and late summer compared to early summer, although during all summer months these air masses are relatively infrequent compared to continental air masses. Only the temperature analyses of Bryson (1966) also display a dominance of continental over maritime or transitional air masses in summer.

e. Autumn (September-November)

Based on the results of this study, the dominant air masses over northwest Ohio during autumn differ considerably from those of the other seasons. The trajectory analyses suggest that Arctic, Canadian, Pacific, and Southwest air masses are less frequent in autumn compared to the other seasons. In fact, the north-northwesterly airflow corridor, the source of Arctic air

masses, all but disappears in September. The southerly, southeasterly, easterly, and northeasterly corridor, source of tropical and Atlantic air masses, are more important in autumn compared to the other seasons, especially in September and October. These results indicate a greater diversity of air mass types in autumn compared to the other seasons.

These results generally concur with those of previous authors. Schwartz (1982;1991) and Schwartz et al. (1985) found that continental, Pacific, dilute tropical and transitional air masses are all common during autumn. Bryson's (1966) results also suggest a variety of air mass type during autumn. He found that, as in summer, the mean confluence zone was located to the north of northwest Ohio in early autumn and over northwest Ohio in late autumn. Thus, his tropical air masses from the Gulf of Mexico are dominant in early autumn, whereas both Pacific and "return polar" air are frequent in late autumn. In contrast to the other studies, Wendland and Bryson (1981) found that the primary air mass source region during autumn is the nearby Ohio Valley.

CHAPTER V

CONCLUSIONS

This study employed GIS-based tools to prepare an air mass climatology for northwest Ohio based on 5-day back trajectories. This research improves our understanding of the air mass climatology of northwest Ohio, and also provides potentially useful tools for constructing general purpose airflow climatologies, beneficial in a broad range of disciplines such as entomology, pathology, and atmospheric chemistry. The major findings of the study can be summarized as follows:

1) The monthly unadjusted and adjusted grid cell frequencies of the 5-day back trajectory nodes illuminated numerous airflow corridors influencing northwest Ohio. These airflow corridors have both geographic and monthly preferences and are the means by which air masses are transported to the study site. The major airflow corridors include:

> North-northwesterly corridor. The most distinct airflow corridor, present in all months except September and October, is the north-northwesterly corridor. This corridor, evident as a long, narrow band of trajectory nodes, follows a north-northwesterly axis that skirts the western shore of Hudson Bay in Canada. There is little change in the location of the airflow corridor during the course of the year, although there are considerable changes in extent (i.e., length) from month to

month. Beginning in February and March, the north-northwest corridor becomes particularly well-defined, and at its greatest extent reaches into the Canadian Arctic archipelago. The well-defined north-northwest airflow corridor continues through August, although the length of the corridor decreases from March to August. In August/September, the north-northwest airflow pattern almost disappears. The corridor strengthens in November, only to diminish again in December and January. Since the corridor extends well into the Canadian arctic during many months, the air masses associated with this corridor were termed "Arctic" air masses. The well-defined north-northwesterly airflow corridor, with its distinct location and persistence in almost all months, has important climatological consequences for northwest Ohio as a source of cold dry air in all seasons of the year.

Northwesterly corridor. A northwesterly corridor is present in all months. This corridor is much more spatially dispersed than the north-northwesterly corridor. The northwesterly corridor displays considerable variations in extent and is strongest in February-May and again in November-December. It also has a fairly strong presence in June-September, although the spatial extent is smaller compared to the other months. This corridor originates in western Canada from a fan-shaped region extending from Great Slave Lake

south-southwestward to southern British Columbia. The air masses associated with this corridor were termed "Canadian".

Westerly corridor. A westerly airflow corridor is also evident in many months. However, it is best defined in December-March. During these months, the westerly corridor usually extends beyond the states of Washington and Oregon over the Pacific Ocean. This corridor also encompasses source regions in the lee of the Rocky Mountains where there frequently appeared to be clustered trajectory nodes. The westerly corridor is also important in April-August, but the spatial extent of the trajectory is less during the warmer months. Trajectories in this corridor tended to be longer, especially in December-March, than for the northwesterly and north-northwesterly airflow corridors. The air masses associated with this corridor were termed "Pacific".

Southwesterly corridor. Although relatively dispersed in all months, a southwesterly corridor is best defined in December-April, and again in June-September. Trajectories associated with the southwesterly corridor tended to be longer than those for the other corridors, with the exception of the westerly corridor. The -120 hour trajectory nodes in this corridor typically originate over the Pacific Ocean off the coasts of California and northern Mexico, extend through the southwest U.S., and intersect the primary westerly corridor in the central Rocky Mountains or to the lee of the mountains in the Central Plains. The

source region name, "Southwest", was given to air masses from this corridor.

Northeasterly corridor. A northeasterly airflow corridor is most prominent in October-January. However, plots of the actual trajectories revealed that the majority of the trajectories within this airflow corridor originated from the west and then curved anticyclonically in the area of southeastern Ontario and western Quebec before terminating in northwest Ohio. This was particularly the case in autumn and early winter. A few of the trajectories truly originated to the northeast of the study site, as evidenced by the percentages in Table 5, and the air masses associated with these trajectories were termed "Atlantic". The air masses associated with the recurving trajectories were not given a name, although most of these air masses appeared to originate along either the north-northwesterly, northwesterly, or westerly corridors. Future research might focus on the synoptic events or conditions that cause trajectories that originate to the west of the study region to curve anticyclonically over eastern Canada and to arrive at northwest Ohio with an easterly orientation.

Easterly corridor. There is some evidence in August and September and perhaps again in January of an easterly corridor. The -120 hour trajectory nodes for this corridor extended just off the eastern coast

of the U.S. from Massachusetts to New Jersey and over the Atlantic Ocean. The name given to the air masses associated with this infrequently occurring corridor was "Atlantic".

Southeasterly and southerly corridors. Southeasterly and southerly corridors are also relatively infrequent, but occur mostly in July-October. The southeasterly corridor extends over the Atlantic Ocean off the southeastern U.S. coast during early winter, and then again in May, July, September, and October. In summer, when generally the length of trajectories is smaller, the southeasterly corridor was frequently confined to the southeastern states of the U.S. The southerly airflow corridor included trajectory nodes which extended to the south of the study site, sometimes reaching over the Gulf of Mexico. The air mass name given to the southeasterly and southerly corridors was "Tropical".

2) The results of the air mass climatology presented here indicate a dominance of Arctic, Canadian, Pacific and Southwest air masses in all seasons for northwest Ohio. This overwhelming dominance of air masses from source regions in the western half of the compass was expected, given the location of northwest Ohio within the main belt of the Northern Hemisphere mid-latitude westerlies.

3) The monthly analysis employed here uncovered considerable with-season variability that was not found in previous studies that for the most part were limited to seasonal analyses.

4) The type of methodology has a large influence on the results of an air mass climatology. The results of this study agreed best with earlier studies that employed an airflow-based methodology rather than with the earlier studies that employed temperature and moisture-based criteria to identify air masses. For example, the airflow-based studies (including this author's) found westerly and west-southwesterly airflow and air masses of Pacific origin to be most important in winter, while the temperature-based studies identified continental polar air mass types to be most important. In general, this research found considerably less evidence of Tropical air masses in northwest Ohio in all seasons than previous authors.

5) The GIS approach used in this study for analyzing the airflow trajectory nodes was extremely useful in illuminating important airflow corridors and air mass source regions for the study site. The GIS streamlined the process of map production, as well as the preparation and analysis of the trajectory node data. The adjusted frequency maps were more effective to use than the unadjusted maps since the concentration of nodes at the terminus on the unadjusted maps was often distracting. Future enhancements could include the conversion of the grid cell frequencies to a probability surface. These probability surfaces could then be contoured or viewed in a three-dimensional perspective with airflow corridors

appearing as ridges.

6) In this thesis, the trajectory frequency node data were transformed from latitude and longitude coordinates to the more equal area Transverse Mercator projection using nearest neighbor resampling methods. With this method, it is likely for the frequency counts to be altered. An alternative method would be to project the trajectory vectors before overlaying an equal area grid. Additionally, a coarser grid cell size for the overlay grid may be produce a "smoother" distribution of the trajectory node frequency counts.

7) The 24-hour weighted mean centers (i.e., average trajectories) proved not to be meaningful in understanding air mass source regions. In fact, they were frequently misleading since they often did not fall along any of the major airflow corridors. For example, in April the average trajectory on the adjusted frequency map represented a combination of two corridors. For Days 1 and 2, the average trajectory represented the northwesterly airflow corridors, but by Day 5 the location of the weighted mean center was predominately influenced by the longer southwesterly trajectories.

8) The quadrant percentages (Tables 4 and 5) were a useful supplement to the frequency maps as a means of providing a quantitative measure of the trajectory node data. They could not be used by themselves as a basis for an air mass climatology, however, since important airflow corridors are masked by compass quadrant summaries. For example, the northwesterly and the north-northwesterly airflow corridors would have been indistinguishable using only the quadrant

percentages. Perhaps a finer division of the compass would yield more meaningful results.

9) The length of the time period of the data set probably was sufficient for identifying the major airflow corridors. However, future research employing this methodology may benefit from a longer time period than ten years, as well as one which encompasses the more recent period of 1986 through the present, given the recent attention focused on global warming. This methodology could also be applied to trajectories calculated from output from General Circulation Models and regional climate models. Comparison of the analyses for a perturbed and a control climate could provide useful insights on possible changes in airflow corridors with greenhouse-induced warming.

BIBLIOGRAPHY

Achtemeier, G. L. (1979) Evaluation of operational objective streamline methods. *Monthly Weather Review*, vol. 107, 198-206.

Ahrens, C. Donald (1994) *Meteorology Today*, West Publishing Company.

Air Resources Laboratories, NOAA. *The ARL HY-SPLIT model.* [Online] Available http://www.arl.noaa.gov/ready.html, October, 1997.

Artz, R., Pielke R., Galloway J. (1985) Comparison of the ARL/ATAD constant level and the NCAR isentropic trajectory analyses for selected case studies. *Atmospheric Environment*, vol. 19, 47-63.

Ashbaugh L. L., Malm W. C., Sadeh W. Z. (1984) A residence time probability analysis of sulfur concentrations at Grand Canyon National Park. *Atmospheric Environment*, vol. 19, 1263-1270.

Barry, R. G. (1967) Seasonal location of the Arctic front over North America. *Geographical Bulletin*, vol. 9, no. 2, 79-95.

Bergeron, T. (1928) Uber die dreidimensional verknupfende Wetteranalyse, *Geofysiske Publikationaer*, vol. 5, no. 6.

Bergeron, T. (1930) Rechtlinien einer dynamischen Klimatologie, *Met. Z.*, 246-262.

Bjerknes, V. (1921) On the dynamics of the circular vortex with applications to the atmosphere and the atmospheric vortex- and wave-motions. *Geofysiske Publikationer*, vol. 2, no. 4.

Borchert, J. R. (1950) The climate of the central North American grassland. *Annals of the Association of American Geographers*, vol. XL, no. 1, 1-39.

Bryson, R. A. (1966) Air masses, streamlines, and the boreal forest. *Geographical Bulletin*, vol. 8, no. 3, 228-269.

Brunnschweiler, D. H. (1952) The geographic distribution of air masses in North America. *Vierteljahrsschrift der Naturf. Gesellschaft in Zurich*, vol. 97, 42-49.

Carlson, J. D., Whalon, M. E., Landis, D. A., Gage, S. H. (1992) Springtime weather patterns coincident with long-distance migration of potato leafhopper into Michigan. *Agricultural and Forest Meteorology*, vol. 59, 183-206.

Clark, J. F., Clark, T. L., Ching, J., Haagenson, P. L., Husar, R. B., Patterson, D. E. (1983) Assessment of model simulation of long-distance transport. *Atmospheric Environment,* vol. 17, 2449-2462.

Clark, W. A., Hosking, P. L. (1986) *Statistical Methods for Geographers,* John Wiley & Sons, New York.

Comrie, A. C. (1994) Tracking ozone: air-mass trajectories and pollutant source regions influencing ozone in Pennsylvania forests. *Annals of the Association of American Geographers*, vol. 84(4), 635-651.

Corcoran, W. T. (1987) Air mass climatology, in Oliver, J. and Fairbridge, R. (eds), *The Encyclopedia of Climatology*, Van Nostrand Reinhold, New York, 22-27.

Danielsen, E. F. (1961) Trajectories: isobaric, isentropic and actual. *Journal of Meteorology*, vol. 18, 479-486.

Davis J. M. and Main C. E. (1986) Applying atmospheric trajectory to problems in epidemiology. *Phytopathology*, vol. 76, 490-497.

Dayan, U. (1986) Climatology of back trajectories from Israel based on synoptic analysis. *Journal of Climate and Applied Meteorology*, vol. 25, 591-595.

Department of Commerce (1968) *The Climatological Atlas of the United States.*
Draxler, R. R. (1992) Hybrid single-particle Lagrangian integrated trajectories (HY-SPLIT). NOAA Tech. Memo. ERL-ARL 195.

Eastman, J. R. (1992) *IDRISI version 4.0*, Clark University, Grad. School of Geography, Worcester, MA.

Eliassen, A. (1980) A review of long-range transport modeling. *Journal of Applied Meteorology*, vol. 19, no. 3, 231-240.

Haagenson, P. L., Kuo, Y., Skumanich, M. (1987) Tracer verification of trajectory models. *Journal of Climate and Applied Meteorology*, vol. 26, 410-426.

Harman, J. R. (1987) Mean monthly North American anticyclone frequencies, 1950-79. *Monthly Weather Review,* vol. 115, 2840-2848.

Harman, J. R. (1991*) Synoptic Climatology of the Westerlies: Process and Patterns.*
Association of American Geographers Resource papers in geography no. 11.

Harris, J. M. (1982) The GMCC atmospheric trajectory program. NOAA Tech. Memo. ERL-ARL-116, 30 pp.

Harris, J. M. (1992) An analysis of 5-day midtropospheric flow patterns for the South Pole: 1985-1989. *Tellus 44B*, 409-421.

Harris, J. M. and Kahl, J. D. (1990) A descriptive atmospheric transport climatology for the Mauna Loa Observatory, using clustered trajectories. *Journal of Geophysical Research*, vol. 95, 13651-13667.

Harris, J. M. and Kahl, J. D. (1994) Analysis of 10-day isentropic flow patterns for Barrow, Alaska: 1985-1992. *Journal of Geophysical Research*, vol. 99, (D12), 25845-25855.

Harris, J. M. and Oltmans, S. J. (1997) Variations in tropospheric ozone related to transport at American Samoa. *Journal of Geophysical Research*, vol. 102, (D7), 8781-8791.

Heffter, J.L., Taylor, A.D., Ferber, G.J. (1975) A regional-continental scale transport, diffusion, and deposition model. NOAA Tech. Memo. ERL-ARL-50, Silver Spring, MD, 28 pp.

Heffter, J. L. (1981) Air Resources Laboratories Atmospheric Transport and Dispersion Model (ARL-ATAD), NOAA Tech. Memo. ERL ARL-81, Silver Spring, MD, 17 pp.

Henmi, T. and Bresch, J. T. (1985) Meteorological case studies of regional high sulfur episodes in the western United States. *Atmospheric Environment*, vol. 19(11), 1783-1796.

Hoecker, W. H. (1977) Accuracy of various techniques for estimating boundary-layer trajectories. *Journal of Applied Meteorology,* vol. 16, 374-383.

Jenne, R. L. (1975) *Data sets for meteorological research.* NCAR Tech. Note NCAR-TN/IA-111, 194 pp.

Kahl, J. D. and Samson, P. J. (1988) Trajectory sensitivity to rawinsonde data resolution. *Atmospheric Environment,* vol. 22(7), 1291-1299.

Kuo, Y., Skumanich, M., Haagenson, P. L., Chang, J. S. (1985) The accuracy of trajectory models as revealed by the observing system simulation experiments. *Monthly Weather Review,* vol. 113(11), 1852-1867.

Malm W. C., Gebhart K. A., Henry R. C. (1990) An investigation of the dominant source regions of fine sulfur in the western United States and their areas of influence. *Atmospheric Environment*, vol. 24, 3047-3060.

Merrill, J. T. (1994) Isentropic airflow probability analysis. *Journal of Geophysical Research*, vol. 99(D12), 25881-25889.

Miller, J. M. (1981a) A five-year climatology of five-day back trajectories from Barrow, Alaska. *Atmospheric Environment*, vol. 15, 1401-1405.

Miller, J. M. (1981b) A five-year climatology of back trajectories from the Mauna Loa Observatory, Hawaii. *Atmospheric Environment*, vol. 15, 1553-1558.

Miller, J. M. and Harris, J. M. (1985) The flow climatology to Bermuda and its implications for long-range transport. *Atmospheric Environment*, vol. 19, 409-414.

Moore, J.T. (1993) Isentropic analysis and interpretation: operational applications to synoptic and mesoscale forecast problems. National Weather Service Training Center. Kansas City, Missouri.

Oliver, J. E. (1970) A genetic approach to climate classification. *Annals of the Association of American Geographers*, vol. 60, 615-637.

Pack, D.H., Ferber, G., Heffter, J., Telegadas, K., Angell, J., Hoecker, W., Machta, L. (1978) Meteorology of long-range transport. *Atmospheric Environment*, vol. 12, 425-444.

Poirot R. L. and Wishinski P. R. (1986) Visibility, sulfate, and air mass history associated with the summertime aerosol in Northern Vermont. *Atmospheric Environment*, vol. 20, 1457-1469.

Robinson, A. H., Sale, R., Morrison, J. (1978) *Elements of Cartography*, 4th ed., John Wiley & Sons, New York.

Schwartz, M. D. (1982) *Air mass climatology of the north central United States.* Master's Thesis, Department of Geography, Michigan State University, East Lansing, MI.

Schwartz, M. D. (1991) An integrated approach to air mass classification in the north central United States. *Professional Geographer*, vol. 43, 77-91.

Schwartz, M. D. (1995) Detecting structural climate change: an air mass-based approach in North Central United States, 1958-1992. *Annals of the Association of American Geographers,* vol. 85(3), 553-568.

Schwartz, M. D., Harman, J., Marotz, G. (1985) Air Mass Characteristics over the North Central United States. *Geographical Perspectives,* no. 56, 13-26.

Schwartz, M. D., Skeeter, B. R. (1994) Linking air mass analysis to daily and monthly mid-tropospheric flow patterns. *International Journal of Climatology,* vol. 14, 439-464.

Scott, R. W. and Achtemeier, G. L. (1987) Estimating pathways of migrating insects carried in atmospheric winds. *Environmental Entomology*, vol. 16, 1244-1254.

Showalter, A. K. (1939) Further studies of American air mass properties. *Monthly Weather Review*, July, 204-217.

Stark, L. P. (1965) Positions of monthly mean troughs and ridges in the Northern Hemisphere, 1949-1963. *Monthly Weather Review,* vol. 93, 705-720.

Trenberth, K. E. and Olson, J. G. (1988) An evaluation and intercomparison of global analyses from the National Meteorological Center and the European Centre for Medium Range Weather Forecasts. *American Meteorological Society Bulletin,* vol. 69(9), 1047-1057.

Wallace, J.M. and Hobbs, P.V. (1977) *Atmospheric Science (an introductory survey),* Academic Press, New York and London.

Warner, T. T., Fizz, R. R., Seaman, N. L. (1983) A comparison of two types of atmospheric transport models - use of observed winds versus dynamically predicted winds. *Journal of Climate and Applied Meteorology,* vol. 22, 394-406.

Wendland, W. M. and Bryson, R. A. (1981) Northern Hemisphere airstream regions. *Monthly Weather Review*, vol. 109, 255-270.

Wendland, W. M. and McDonald, N.S. (1986) Southern Hemisphere airstream climatology. *Monthly Weather Review,* vol. 114, 88-94.

Wolff, G. T., Morrissey, M., Kelly, N. (1984) An investigation of the sources of summertime haze in the Blue Ridge Mountains using multivariate statistical methods. *Journal of Climate and Applied Meteorology*, vol. 23, 1333-1341.

Willett, H. C. (1933) *American air mass properties*, Papers in physical oceanography and meteorology published by M.I.T. and Woods Hole Oceanographic Institution, vol. 2, no. 2.

Winkler, J. A., Harman, J. R., Waller, E. A., Brown, J. T. (1996) Climatological characteristics of springtime lower tropospheric airflow over central and eastern North America. *International Journal of Climatology*, vol. 16, 739-755.